NAVAL POSTGRADUATE SCHOOL

MONTEREY, CALIFORNIA

THESIS

OPTIMAL ORBIT MANEUVERS WITH ELECTRODYNAMIC TETHERS

by

Andrew F. Carlson

June 2006

Thesis Advisor:	I. Michael Ross
Co-Advisor:	Don A. Danielson

Approved for public release; distribution is unlimited

THIS PAGE INTENTIONALLY LEFT BLANK

REPORT DOCUMENTATION PAGE

Form Approved OMB No. 0704-0188

1. AGENCY USE ONLY *(Leave blank)*	**2. REPORT DATE** June 2006	**3. REPORT TYPE AND DATES COVERED** Master's Thesis

4. TITLE AND SUBTITLE: Optimal Orbit Maneuvers with Electrodynamic Tethers

5. FUNDING NUMBERS

6. AUTHOR(S) LCDR Andrew F. Carlson, USN

7. PERFORMING ORGANIZATION NAME(S) AND ADDRESS(ES)
Naval Postgraduate School
Monterey, CA 93943-5000

8. PERFORMING ORGANIZATION REPORT NUMBER

9. SPONSORING /MONITORING AGENCY NAME(S) AND ADDRESS(ES)
N/A

10. SPONSORING/MONITORING AGENCY REPORT NUMBER

11. SUPPLEMENTARY NOTES The views expressed in this thesis are those of the author and do not reflect the official policy or position of the Department of Defense or the U.S. Government.

12a. DISTRIBUTION / AVAILABILITY STATEMENT
Approved for public release; distribution is unlimited

12b. DISTRIBUTION CODE

13. ABSTRACT (maximum 200 words)

Electrodynamic tethers can be employed to effect spacecraft orbital maneuvering outside of Keplerian motion without incurring the mass penalty of traditional propulsion systems. Recently, several studies have been conducted to establish a framework for guidance and control of such orbit maneuvers, including the optimization of a particular maneuver, the orbit transfer. This thesis provides an overview of the concept of electrodynamic tether employment, summarizes research in the field, and catalogues recent proposals. Two minimum-time orbit transfer problems are considered - an orbit raising and a deorbit problem. Both formulations use an identical set of initial conditions for the spacecraft. In the case of the orbit raising problem formulation, the terminal manifold requires an increase in semimajor axis and return to initial eccentricity and inclination values. Other orbital elements are unconstrained. For the deorbit case, optimal control is developed for a minimum time decrease in semimajor axis; the remaining orbital elements are unconstrained. The totality of optimality conditions for both cases of using electrodynamic tethers to maneuver from an initial orbit is examined. Observations and recommendations for future work are presented in the conclusions.

14. SUBJECT TERMS Electrodynamic Tethers, Orbit Transfer, Optimal Orbit Maneuvers, DIDO	**15. NUMBER OF PAGES** 85
	16. PRICE CODE

17. SECURITY CLASSIFICATION OF REPORT	**18. SECURITY CLASSIFICATION OF THIS PAGE**	**19. SECURITY CLASSIFICATION OF ABSTRACT**	**20. LIMITATION OF ABSTRACT**
Unclassified	Unclassified	Unclassified	UL

NSN 7540-01-280-5500

Standard Form 298 (Rev. 2-89)
Prescribed by ANSI Std. 239-18

THIS PAGE INTENTIONALLY LEFT BLANK

Approved for public release; distribution is unlimited

OPTIMAL ORBIT MANEUVERS WITH ELECTRODYNAMIC TETHERS

Andrew F. Carlson
Lieutenant Commander, United States Navy
B.S., United States Naval Academy, 1995

Submitted in partial fulfillment of the
requirements for the degree of

MASTER OF SCIENCE IN ASTRONAUTICAL ENGINEERING

from the

NAVAL POSTGRADUATE SCHOOL
June 2006

Author: Andrew F. Carlson

Approved by: Dr. I. Michael Ross
Thesis Advisor

Dr. Don A. Danielson
Co-Advisor

Dr. Anthony J. Healy
Chairman, Department of Mechanical and Astronautical Engineering

THIS PAGE INTENTIONALLY LEFT BLANK

ABSTRACT

Electrodynamic tethers can be employed to effect spacecraft orbital maneuvering outside of Keplerian motion without incurring the mass penalty of traditional propulsion systems. Recently, several studies have been conducted to establish a framework for guidance and control of such orbit maneuvers, including the optimization of a particular maneuver, the orbit transfer. This thesis provides an overview of the concept of electrodynamic tether employment, summarizes research in the field, and catalogues recent proposals. Two minimum-time orbit transfer problems are considered - an orbit raising and a deorbit problem. Both formulations use an identical set of initial conditions for the spacecraft. In the case of the orbit raising problem formulation, the terminal manifold requires an increase in semimajor axis and return to initial eccentricity and inclination values. Other orbital elements are unconstrained. For the deorbit case, optimal control is developed for a minimum time decrease in semimajor axis; the remaining orbital elements are unconstrained. The totality of optimality conditions for both cases of using electrodynamic tethers to maneuver from an initial orbit is examined. Observations and recommendations for future work are presented in the conclusions.

THIS PAGE INTENTIONALLY LEFT BLANK

TABLE OF CONTENTS

LIST OF FIGURES

LIST OF TABLES

THIS PAGE INTENTIONALLY LEFT BLANK

ACKNOWLEDGMENTS

Exceptional thanks are due to Dr. Ross for sharing his insights and methodology. There really are only a very few key ideas, one of which is being able to differentiate between the wrong answer and the right answer to a wrong question. I am indebted to you for pearls such as this.

Extreme gratitude is for Dr. Danielson, a willing partner in this effort at the eleventh hour. To Dr. Chirold Epp, many thanks for introducing me to the world of astrodynamics. Many thanks also go to CAPT Al Scott for top cover and latitude to complete this work.

Thanks are also due to Dr. Rustan, CAPT Frank Garcia, and Steve Mauk, who each in his own way encouraged my sense of adventure in challenging the feasible set of research.

To my laboratory neighbors and sincerely professional scientists Pooya Sekhavat, Kevin Bollino, and Ron Moon: thanks for sharing space and assistance throughout this endeavor.

Heartfelt thanks go to my fellow officers of the NPS 2005 graduating class of space engineers. "Many hands make light work." I consider our association and friendship a privilege of the highest order.

Lastly, I thank my new wife, Heidi Maria, for her loving support, and God Almighty for seeing me through to completion. He is faithful indeed.

THIS PAGE INTENTIONALLY LEFT BLANK

I. INTRODUCTION

A. PURPOSE

This thesis is presented to achieve a threefold goal, namely, to summarize research and development efforts in the area of electrodynamic tethers, to validate recent optimization of a particular electrodynamic tether application, and to suggest future research efforts and program requirements for continued development in the field.

B. MOTIVATION

In spacecraft engineering, the fact that increased mass and/or propellant means increased program dollars required is not lost on anyone: professors, scientists, or space enthusiasts alike. The hard and fast rules of Newton and Kepler, though developed hundreds of years ago are still as applicable today in the space age, where space launch is not even restricted to the government or industrial sector. It is no wonder that alternatives to standard fuel and mass expenditures in space lift and space travel are continually in focus. In this regard, the electrodynamic tether as a research area is no different than the latest theories for modification to standard chemical propellants, e.g. hydrazine, or ongoing propulsion studies such as the VASIMIR rocket engine. These research efforts all seek to decrease mass fractions while increasing propellant availability and efficiency for on-orbit maneuvering. With respect to orbital maneuvering using electrodynamic tether, however, traditional understanding of feasible orbital maneuvers is dwarfed by the new range of feasible movements seemingly for "free." The idea that electrodynamic tethers could provide low thrust for propellantless orbital maneuvers opens up a completely new set of satellite maneuvers. From a cost/risk management perspective, we cannot afford to ignore the immeasurable opportunities that tether-based maneuvering provides. This viewpoint is a fundamental motivator in this study.

C. DEFINITIONS

1. Coordinate Systems

The initial part of the consolidation effort with summarizing research lies in establishing common terminology for coordinate systems and variables used. The inertial reference system depicted in Figure 1 is used to illustrate classical orbital elements defined in the next section. The coordinate system used is the Geocentric Celestial Reference Frame (GCRF), which is the standard Earth centered inertial reference system, with the I axis towards the first point of Ares at a specific epoch, K towards the North Pole, and the J axis completing the right-hand system, commensurate with Earth rotation. Portions of two other coordinate systems are observable from the figure: the perifocal (PQW) and satellite coordinate (RSW) systems, both of which are satellite based rather than Earth centered. Whereas the PQW coordinate system is useful for in-orbit reference or satellite observation processing[1], our purposes are more easily suited by use of the RSW coordinate system which relies on satellite radial and tangential directions of motion with respect to the orbit plane. As discussed in Bate, et al[2], the RSW coordinate system also provides ease of differentiation when manipulating the dynamic equations of satellite motion using variation of parameters. These dynamic relationships are discussed further under problem formulation in Chapter IV.

2. Variables

The principal variables used in our model follow the classical orbital elements and their time rate of change with respect to externally applied perturbation accelerations, namely low-thrust propulsive force initiated via a control current through the tether. The dynamic relationships and physical constraints are more thoroughly developed in following chapters. For our purposes, the six classical orbital elements that uniquely describe a satellite are used as the state vector in our problem formulation.

---

[1] David A. Vallado. *Fundamentals of Astrodynamics and Applications, 2nd ed.* 2001: Microcosm Press, El Segundo, CA, pp. 158-165.

[2] Roger R. Bate, Donald D. Mueller, and Jerry E White. *Fundamentals of Astrodynamics*. 1971: Dover Publications, Inc, New York. pp. 397-398.

a = semimajor axis	e = eccentricity
i = inclination	Ω = right ascension of ascending node
ω = argument of perigee	ν = true anomaly

The first two variables are principal in describing the two-dimensional orbit representation, namely the ellipse size and shape, respectively. As depicted in Figure 1 on the following page, the next three classical orbital elements describe an aspect of satellite position in orbit with respect to an Earth centered frame. Specifically, inclination shows the angle between the vector normal to the orbit plane and the polar or K axis. The right ascension of the ascending node as depicted shows the angle between the I axis (which at the vernal equinox is a line containing both the earth and the sun) and the line of nodes (***n*** vector) at the intersection of the equatorial plane with the orbit plane. Finally the argument of perigee describes the angle between the ellipse periapsis and the equatorial plane and is useful for determining the latitude of perigee, the closest point the satellite comes to the earth. The final state variable, true anomaly, describes the angular position of the body within the orbit plane related to periapsis, or the P axis in the perifocal coordinate system.

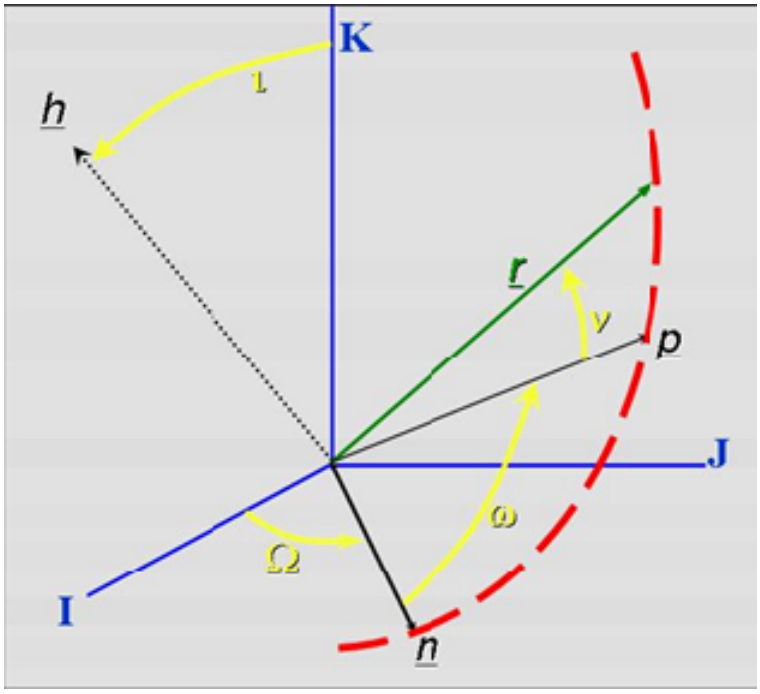

Figure 1. Coordinate Axes and Variables in use

These six variables are the classical orbital elements employed in the problem formulation. Other works cited have used variations on the primary state vector that were not entertained for our purposes, however some attention is later given to these variations in a discussion of recent research efforts and finally in concluding recommendations for follow-on work.

Other variables of interest, for expression simplification and computation include the following: p = semi-latus rectum (or semiparameter), h = orbit angular momentum, and r = orbit radius. Their relationships to the state variables are defined later in problem formulation.

3. Notation

Wherever required, a standardized notation is implemented for consistency. Vectors are discernable from scalars as underlined variables. Subscripts follow conventional nomenclature, in that U and L stand for upper and lower bounds, respectively, o and f are similarly used for initial and final conditions of terms, respectively. Dots signify time derivatives of variables.

4. Constants

Computational constants routinely employed in this work include the gravitational parameter μ, and the radius of the Earth, R_e. Both constants were used as in Vallado according to table 1 on the following page. Care is taken not to confuse the gravitational parameter with the permeability constant μ_o The Earth magnetic dipole moment can be combined with the permeability constant to establish the quantity $\mu_m = \mu_o \mathbf{m_d}$, which has units Tesla-$m^3$.

Symbol	Constant	Value	Units
μ	Gravitational Parameter	$3.986004415 \times 10^{14}$	m^3/s^2
$\mathbf{R_e}$	Earth Radius	6.3781363×10^{6}	m
μ_o	Permeability constant	$4\pi \times 10^{-7}$	Henry/m
$\mathbf{m_d}$	Earth magnetic dipole moment	8.1×10^{22}	m^2Amp

Table 1. Computational Constants

This quantity is used in determining the value of the magnetic field at the satellite orbit position. Other parameters in use, e.g. tether length, are generally arbitrary values yet constant in the application and will be discussed during problem formulation.

D. ENVIRONMENT

With parameters and nomenclature established, it is important to briefly describe the area of satellite orbits considered. Electrodynamic tethers as a trade study focus specifically on the low-earth orbit (LEO) regime where the magnetic field of the earth has a significant enough potential for dynamic influence on satellite orbits.

1. Altitude

LEO is typically defined from a few hundred kilometers in altitude out to just over 1000 km. Specific applications of tethers in space, such as the ISS orbit boost objective, obviously focus on a small subset of the LEO environment. This study

considers LEO as between 200 and 1200 km, however the optimization bounds for orbital maneuvering in this problem formulation are set considerably narrower.

2. Drag

Within LEO, atmospheric drag contributes to dynamic perturbations, especially at lower altitudes as atmospheric density increases. The simplest atmospheric drag relationship follows from physics fundamentals[3]: $F_d = \frac{1}{2}\rho K_d A$, where air density ($\rho$), drag coefficient K_d, and area of the satellite A factor into the drag force on the orbiting body. A more complex model follows from Mishne's research in satellite formation control[4], which invokes the Gaussian variation of parameters to produce time rate of change of three classical elements. These relationships are reproduced below for immediate reference.

$$\dot{a} = -(2a/r)(2a-r)\rho V K_d$$
$$\dot{e} = -2(\cos(\nu)+e)\rho V K_d$$
$$\dot{\omega} = -(2\sin(\nu/e)\rho V K_d$$

Note the periodic nature of the eccentricity and argument of perigee derivatives, dependent upon the current value of true anomaly. The expressions above are useful for increasing model fidelity with respect to atmospheric drag, but are not employed in our problem formulation. A sufficient altitude-dependent atmospheric density model is also recommended.

3. Electromagnetic Field

The particular aspect of the LEO environment of most significance to the study of electrodynamic tethers is the influence of the Earth's magnetic field on tethered satellites. Following the simple description of the earth's magnetic field, a dipole is assumed. Several different approximations are available in the literature. Forward and Hoyt's

[3] David Halliday, Robert Resnick, and Jearl Walker. *Fundamentals of Physics, Sixth Ed.*2001: Wiley & Sons, Inc. pp. 104-106.

[4] David Mishne. *Formation Control of Satellites Subject to Drag Variations and J_2 Perturbations*, Journal of Guidance, Control, and Dynamics, Vol. 27. No 4, July-August 2004.

paper on deorbiting space debris apply a constant valued field transverse to both the tether direction and the tangential velocity vector[5]. Tragresser and San[6] and likewise Williams[7] incorporate the Euler-Hill frame construct for the B field, again using an inverse cubic for satellite radius:

$$B_I = -2(\mu_m / \mathrm{R}^3)\sin(\omega + \nu)\sin(i)$$
$$B_J = (\mu_m / \mathrm{R}^3)\cos(\omega + \nu)\sin(i)$$
$$B_K = (\mu_m / \mathrm{R}^3)\cos(i)$$

This model is sufficient and is employed in the problem formulation discussed later; however it does not account for the approximate 11.5^o tilt of the dipole model from the geographic polar axis. Subsequent fidelity improvements include the magnetic field approximation described by Parkinson[8], which relies on an inverse cubic proportion of satellite radius to magnetic field strength. Of course, the best model for the Earth's magnetic field is the standard set in the International Geomagnetic Reference Field (IGRF). Lanoix, et al, use this model in their recent (December 2005) study of electrodynamic force effects on tethered satellites, incorporating the Legendre polynomials and the 1995 IGRF revision.[9]

4. Other Considerations

The oblateness of Earth and the resulting J_2 perturbative effect are not considered for the purposes of this study. Mishne's work on controlling perturbations such as the J_2 effect is germane to models of increased complexity; other research on managing

[5] Robert L. Forward and Robert P. Hoyt, *Terminator Tether TM: A Spacecraft Deorbit Device.* Journal of Spacecraft and Rockets Vol. 37, No. 2, March-April 2000. American Institute of Aeronautics and Astronautics.

[6] Steven G. Tragesser and Hakan San, "Orbital Maneuvering with Electrodynamic Tethers," *Journal of Guidance, Control, and Dynamics*, Vol. 26, No. 5, 2003.

[7] Paul Williams. "Optimal Orbital Transfer with Electrodynamic Tether," *Journal of Guidance, Control, and Dynamics,* Vol. 28, No. 2, March-April 2005. American Institute of Aeronautics and Astronautics.

[8] W.D. Parkinson. *Introduction to Geomagnetism*. Elsevier Science Pub. Co., Inc., New York.

[9] Eric L. M. Lanoix, Arun K. Misra, Vinod J. Modi, and George Tyc. "Effect of Electrodynamic Forces on the Orbital Dynamics of Tethered Satellites". *Journal of Guidance, Control, and Dynamics,* Vol. 28, No. 6, November-December 2005.

oblateness effects will prove ultimately useful in follow-on research, especially as program requirements seek increased model fidelity. For immediate purposes these effects are beyond the scope of the problem formulation as presented.

II. ELECTRODYNAMIC TETHER CONCEPT

A. ORBIT ENVIRONMENT

1. Low Earth Orbit

As discussed in the introductory chapter, electrodynamic tether applications in this problem formulation will remain confined to the LEO environment, i.e., for intents and purposes orbits between 200 and 800 km are considered. This altitude range includes significant spacecraft such as the International Space Station (345 km) and the Space Shuttle (296 km) and allows for sufficient magnitudes of orbit transfer in the analysis.

2. Earth Magnetic Field

The magnetic field as described in the previous chapter is depicted below in Figure 2 with a graphic representation of the field interaction with a tethered satellite. Calculations for the Earth magnetic field, or B field, are not repeated here; though it is appropriate to highlight the nature of the interaction. Specifically, the dipole model of the B field and the according lines of magnetic flux, though variable, do not appreciably change with respect to the B field vector direction. Accordingly, a generalization can be assumed about the vector cross product of current in a tethered satellite and the magnetic field of the earth.

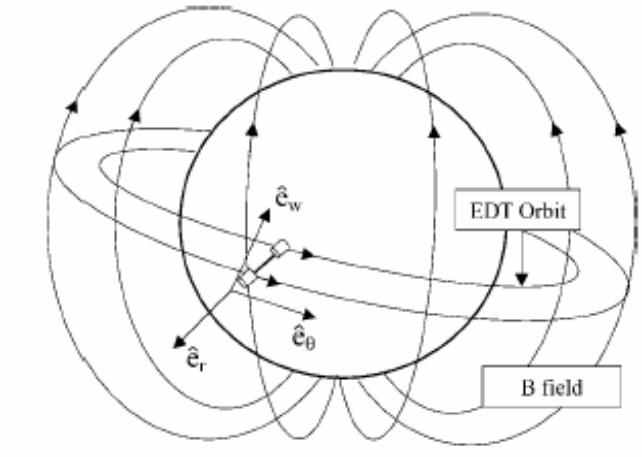

Figure 2. Electrodynamic Tether Concept (from Ref. 6)

That is to say, a consistent observation of the geometry between an orbiting tethered satellite and the B field lines can be made. The Tragresser and San observation below corresponds to Figure 2 above.

> ...because the force is perpendicular to the magnetic field lines, out-of-plane forces cannot be attained when the orbit is coplanar with the magnetic equator, i= 0 deg, and in-plane forces cannot be attained when the orbit is polar with respect to the magnetic field, i= 90 deg.10

Tragresser and San employ a nadir directed tether, fixed towards the Earth, which also eliminates any potential radial acceleration because the force induced from the current in the tether is perpendicular to the tether itself. This zero-libration model, while less complicated to simulate, is disappointing for a particular orbit maneuver such as the orbit boost (or de-boost), in that a radial acceleration component is desirable for faster orbit transfers. Further research efforts incorporate tether librations into the dynamic representation; these will be summarized in the next chapter.

B. PHYSICS

1. Voltage Induction

The electrodynamic tether uses two basic electromagnetic principles to its advantage. The first principle is that of voltage induction, namely, that a voltage is induced when a conductive wire moves through a magnetic field. Created by a separation of charge, the voltage differential present in a tether relies on electrons completing a circuit via the plasma present in the orbital environment. Essentially electrons can exit the tether into the plasma, completing a circuit and thereby enabling the voltage present to drive a current along the tether.

2. Lorentz Force

The second principle of key importance in any electrodynamic tether application concerns the force exerted on a charged particle in an electromagnetic field, named for Dutch physicist H. A. Lorentz. In EDT applications, the principal force involved is the Earth's magnetic field, or <u>B</u> field. The Lorentz Force equation as represented below is

10 S.G. Tragresser and Hakan San, "Orbital Maneuvering with Electrodynamic Tethers," *Journal of Guidance, Control, and Dynamics*, Vol. 26, No. 5, 2003.

used, where F is the induced Lorentz Force, L is the length of tether, and B is the aforementioned Earth magnetic field. I is the current present in the tether; for our application this is the control parameter integral to the optimization process, and will be discussed later.

$$\underline{F} = I(\underline{L} \times \underline{B})$$

3. Application

Experimental work shows that a uniform magnetic field acting on a current-bearing loop of wire normally yields a zero net force. As discussed in Johnson's article[11], a spacecraft tether is not "mechanically attached to the plasma," therefore "the magnetic forces on the plasma currents in space do not cancel the forces on the tether." From Newtonian dynamics, we know that a non-zero net force on any mass defines acceleration, whereby the impetus for electrodynamic tethers originates. If acceleration can be obtained by simply extending a tether of current conducting wire into the Earth's magnetic field, a significant alternative to the consistent problem of propellant vs. mass is possible, as propulsive force is now achievable with little mass penalty (merely the tether and related support equipment). The concept is appealing from an economical point of view but also expands the feasible options for space applications: the answer to the question, "what could be done if a free propulsive force were available for satellite maneuvers?"

C. APPLICATIONS

Indeed, several "free force" applications come to mind once the traditional paradigm of propellant mass fraction and costly space launch is set aside by the electrodynamic tether concept. Brief descriptions of these options follow.

[11] L. Johnson. "The Tether Solution," *IEEE Spectrum*, Vol. 37, No. 7, July 2000. National Aeronautics and Space Administration.

1. Debris Mitigation

The growth of orbital debris in Low Earth Orbit (LEO) is increasing at an alarming rate. There exists over 6000 objects in LEO, and only 300 of these are operational satellites. The remainder is spent upper stages and derelict spacecraft which constitute a major collision hazard for existing and future spacecraft.

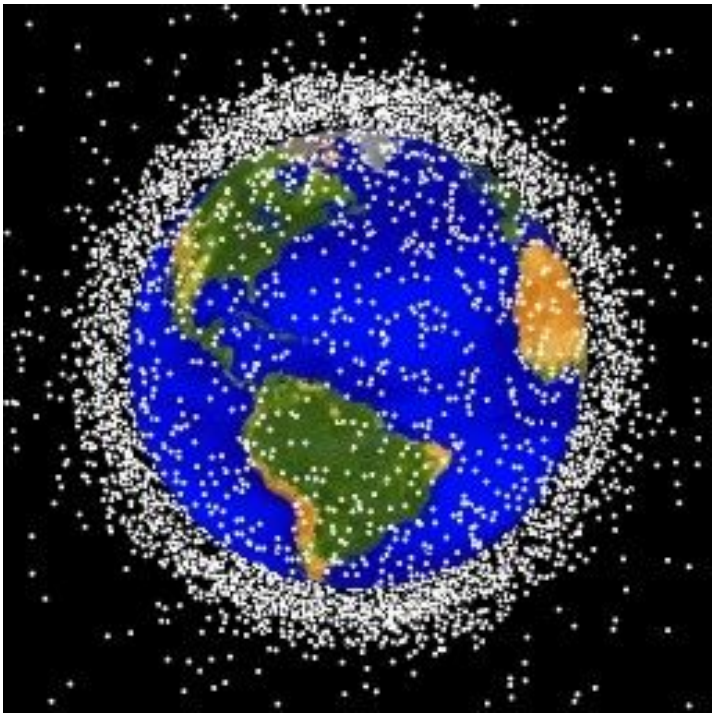

Figure 3. LEO Orbital Debris (from Ref. 5)

Electrodynamic tethers may provide a cost effective means to deorbit existing debris as well as providing for the assured removal of future-launched spent stages and satellites. Several firms are pursuing the idea of tether debris mitigation, and Tethers Unlimited, Inc. appears to have the most viable proposal to date.

The Tethers Unlimited, Inc. *Terminator Tether* ™ concept calls for a terminating tether to be attached to satellites and upper stages prior to launch. The passive system would be comprised of a conducting tether, tether deployer, electron emitter, and associated electronics. When a satellite has reached the end of its operational utility, the terminating tether would be deployed from the satellite. The tether, which would have approximately 2% of the mass of the satellite, would have electrical contact with the

ambient plasma at both ends of the system. This would allow electrical current to be transmitted to and from the existing ionospheric plasma.

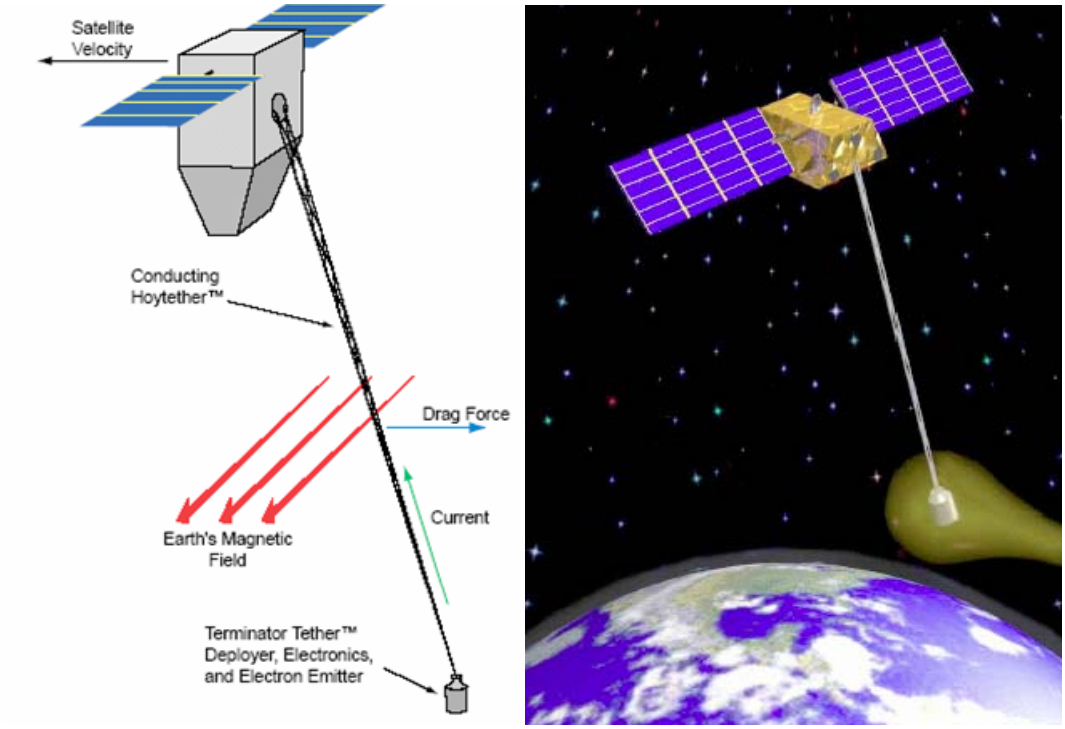

Figure 4. Terminator Tether™ Concept Diagrams (from Ref. 5)

As the deployed tether moves through the Earth's magnetic field, a current will be generated as electrons are collected from the ionosphere and flow down the tether to the electron emitter. The induced current, being defined as the flow of positive charge, would be upward in the direction of the satellite. The interaction between the induced current and the Earth's magnetic field would generate a Lorentz force in the opposite direction of the satellite velocity vector. This drag force would decrease the orbital energy of the satellite and result in more rapid orbit decay, thereby avoiding yet another contribution to "space junk" in LEO.

The use of a system such as the Terminator TetherTM ushers in the question of what mass penalty must be accepted in order to provide a deorbit capability to a

spacecraft at its end of life (EOL). Also in question from a space policy perspective is whether there should be a requirement for deorbiting space lift support equipment such as rocket upper stages or fuel tanks.

Tether mass:	10.0	kg
Shroud:	2.1	kg
Spool Assembly:	5.8	kg
Ejection Mechanism	3.5	kg
Electron Emitter:	1.2	kg
TCU Electronics:	3.7	kg
Tether Anchor	0.15	kg
Total Tether system mass:	26.45	kg

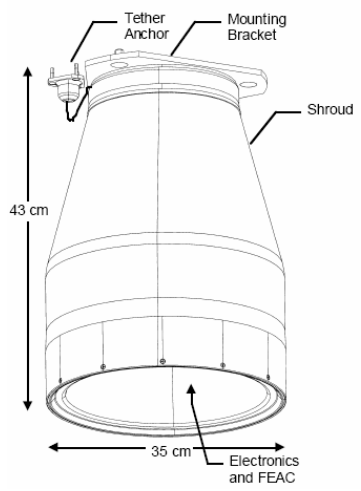

Figure 5. Mass Breakdown and Concept Drawing (from Ref. 5)

Figure 5 above shows the Terminator TetherTM and provides an apportionment of mass for the system. Although the 26.46 kg mass represents about only 2% of the mass of an arbitrary 1000 kg satellite, this is not monetarily trivial. The costs to put 1 kg into LEO can easily approach $10,000/kg, meaning the tether system would cost approximately $260,000. Unless directed by law, most satellite manufacturers are not altruistic enough to pay this penalty to keep space clean for all.

Assuming that these costs for a terminating tether were absorbed, the improvement in deorbit time is significant. As discussed, the functioning of an electrodynamic tether is dependant upon the presence of a magnetic field and ionospheric plasma. Therefore, one would expect the system to be most capable in regions of strong magnetic field lines and high ionic plasma concentrations (i.e. low inclination and low altitude).

Conversely, the region of poorest performance most likely would be at high inclinations (near polar) and high altitudes. This is indeed the conclusion reached through modeling and simulation, as Tragresser and San reported.

Figure 6 depicts the deorbit rate (km/day) of a 1500 kg spacecraft using a tether with a mass of 30 kg and a length of 7.5 km. The influence of inclination and orbiting altitude are easily seen.

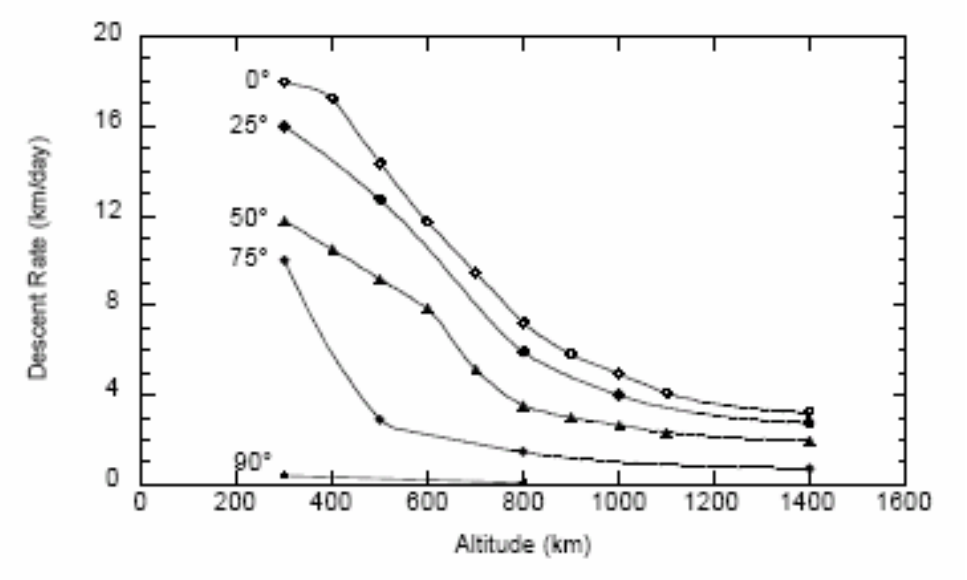

Figure 6. Tether Assisted Satellite Descent Rate (from Ref. 5)

Figure 7 below depicts the time (days) for a tether system to deorbit a satellite, based upon the aforementioned parameters.

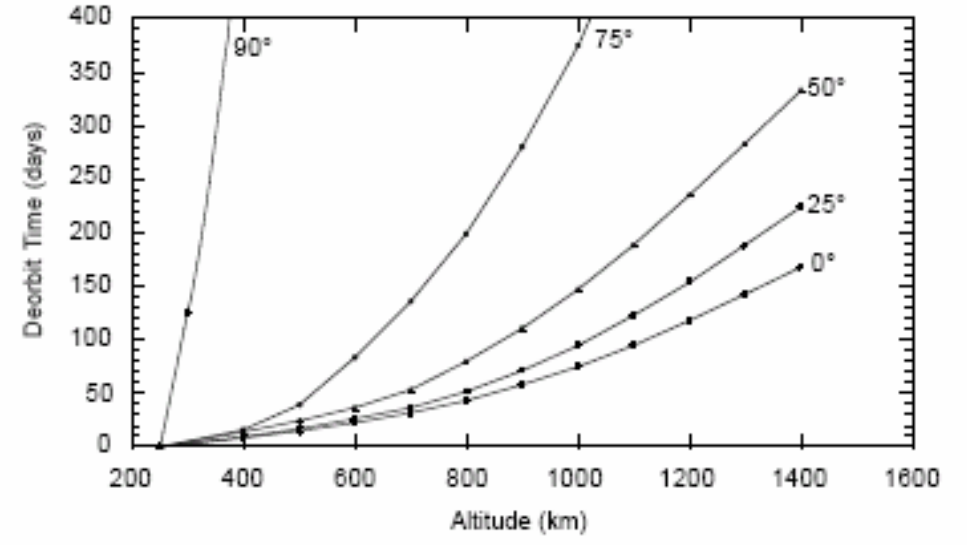

Figure 7. Tether Assisted Satellite Descent Times (from Ref. 5)

The obvious question is how the tether system compares with normal deorbit times which are a function of satellite cross sectional areas and atmospheric drag. The NASA Safety Standard uses an Area-Time Product to compare deorbit capabilities. The employment of a tether system would increase the cross sectional area and thus increase the possibility of a collision; however, it would significantly reduce the amount of time that the system has the potential to be hit. The overall Area-Time Product observable in Figure 8 is significantly less for a tether system when compared to sole reliance on atmospheric drag.

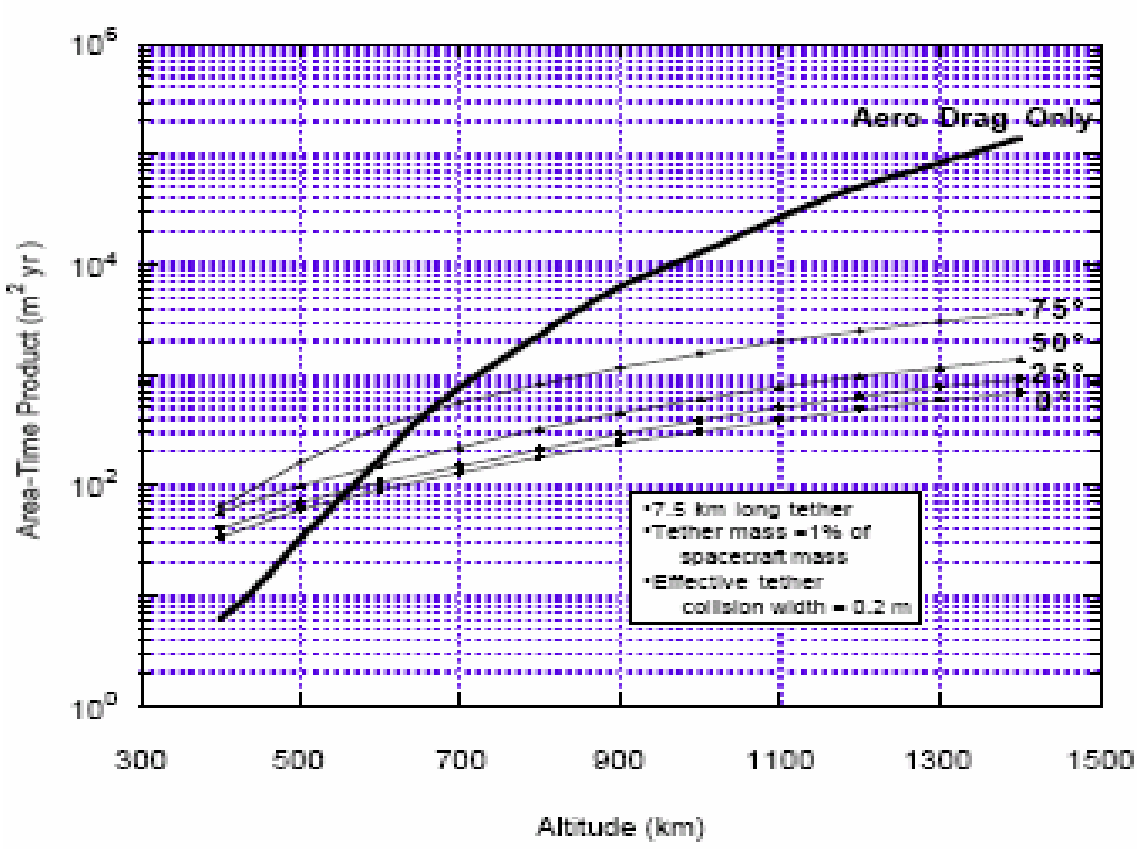

Figure 8. Area-Time Product Comparison (from Ref. 5)

The Area-Time Product for each inclination and altitude presented is considerably better than satellite orbit decay using atmospheric drag alone. It is important to note the logarithmic nature of this graph. The use of a tether system can reduce the Area-Time Product by several orders of magnitude, which equates to deorbit times measured in weeks vice thousands of years. Analysis by Tethers Unlimited, Inc. also provides a summary comparison between tether and non-tether deorbit times, presupposing installation of the Terminator TetherTM on each platform. The data below in Table 2 are based on a tether system mass of 2.5% of overall satellite mass.

Constellation	Altitude (km)	Inclination (degrees)	Deorbit Time, noTT (Derelict)	Initial Orbit Decay Rate (km/day)	Deorbit Time, with Terminator Tether
Orbcomm 1	775	45	100 years	44	11 days
Orbcomm 2	775	70	100 years	11.6	41 days
LEO One USA	950	50	600 years	32	18 days
GlobalStar	1390	52	9,000 years	22.3	37 days
Skybridge	1475	55	11,000 years	18.5	46 days
FaiSat	1000	66	800 years	13.5	45 days
Iridium	780	86.4	100 years	2.1[17]	7.5 months[17]
M-Star	1350	47	7000 years	27	28 days
Celestri	1400	48	9000 years	26	32 days
Teledesic	1350	~85	7000 years	1.7[17]	17 months[17]

Note: All spacecraft are assumed to have an effective drag cross section of 10 m^2.

Table 2. Deorbit Times for Tethered and Non-tethered Systems (from Ref. 5)

2. Orbit Boost (ISS)

The International Space Station (ISS) is one the largest objects ever placed into orbit. Its large cross sectional area and relatively low orbit altitude of 360 km make atmospheric drag a serious issue for keeping the ISS viable. The drag encountered by the station varies between 0.3-1.1N, which results in the station needing reboost every 10 to 45 days. Over the ten year projected operating life of the station, the amount of fuel needed to reboost the ISS will be in excess of 77 metric tons. Using a conservative $7000/lb on orbit cost, the fuel needed to maintain the ISS orbit would be 1.2 billion dollars. A Boeing study completed in 1998 and reported in the spring 2000 Journal of Spacecraft and Rockets showed that “a relatively short tether system, 7 km long, operating at a power level of 5 kW could provide cumulative savings of over a billion

dollars during a 10 year period ending in 2012."[12] Immense cost savings notwithstanding, Vas, et al also advocate the use of an electrodynamic tether for ISS reboost as propellant resupply and STS boost missions are subject to tenuous launch availability. The use of an electrodynamic tether may ameliorate some or all of the aforementioned fuel costs but most certainly could provide capability during periods of resupply inactivity from participating countries in the ISS mission. Tethers Unlimited, Inc. advertises an artist depiction, reproduced in Figure 9 on the following page.

The previous section described the use of an electrodynamic tether to deorbit spent satellites, and now the same principles are used to boost a satellite. The key lies in the direction of current flow. In the deorbit case, the tether had current flow that resulted in a drag force opposite the satellite velocity vector. If it were possible to force this current to flow opposite its desired direction, the outcome would be thrust along the flight path which increase orbital energy and boosts the satellite.

Figure 9. EDT Reboost of ISS (from Ref. 5)

[12] Irwin E. Vas, Thomas J. Kelly, and Ethan A. Scarl, "Space Station Reboost with Electrodynamic Tethers," *Journal of Spacecraft and Rockets*,Vol. 37, No. 2, March-April 2000. American Institute of Aeronautics and Astronautics.

Energy must be provided to overcome the electromotive force (EMF) and force opposite current flow, thus countering the 0.5-1.1 N atmospheric drag experienced by ISS in LEO. An average thrust of 0.5 to 0.8 N could be collected from a 10 km, 200 kg bare (non-insulated) tether (I_{sp} = 0.005 N/kg). The energy which must be supplied to oppose the natural current would be between 5 -10 kW and could be supplied via solar panels. The solar panels that would be necessary to provide this required energy are much more cost effective than the currently projected 1.2 billion dollar fuel costs.

3. Orbit Maneuver

The first two applications discussed above are specific examples of the general application of orbital maneuvering using electrodynamic tethers. The proposition in its entirety is simply whether each of the six classical orbital elements that uniquely define a satellite can be manipulated with a degree of certainty by the use of applied controls in a low-thrust propulsion scheme using electrodynamic tethers.

Tragresser and San showed a simple guidance control scheme to apply current laws developed in the *Tethers in Space Handbook*[13], whereby specific orbital elements can be manipulated with applicable current laws with secular changes to other elements. These current laws are reproduced in Figure 10 for reference. Williams[14] extended their work to model tether librations and subsequently include this libration modeling in determining optimal control for orbit transfer. Lanoix, et al[15], and Hoyt[16] give similar postulation that tether librations should not be seen as instabilities to control but rather opportunities to develop optimal control methodology for maximizing the available perturbation accelerations due to "beneficial" tether librations.

---

[13] M.L. Cosmo and E. C. Lorenzini, *Tethers in Space Handbook, 3rd ed.*, NASA Marshall Space Flight Center Grant NAG8-1160. 1997.

[14] Paul Williams. "Optimal Orbit Transfer with Electrodynamic Tether,: *Journal of Guidance, Control, and Dynamics* Vol. 28, No. 5. 2005 American Institute of Aeronautics and Astronautics.

[15] Eric L. M. Lanoix, Arun K. Misra, Vinod J. Modi, and George Tyc. "Effect of Electrodynamic Forces on the Orbital Dynamics of Tethered Satellites". *Journal of Guidance, Control, and Dynamics,* Vol. 28, No. 6, November-December 2005.

[16] R. P. Hoyt. "Stabilization of Electrodynamic Space Tethers," *Proceedings of Space Technology and Applications International Forum (STAIF-2002)*, American Institute of Physics, Melville NY, 2002, pp. 570-577.

Current law[a]	Orbital element
DC	Semimajor axis
Cos ν	Eccentricity
Sin ν	Argument of perigee
Cos$[2(\nu+\omega)]$	Inclination
Sin$[2(\nu+\omega)]$	Line of nodes

[a]Current laws provide secular change in these corresponding orbital elements.

Figure 10. Current laws and corresponding orbital elements. (from Ref. 6)

Recognizing tether librations as an asset rather than a liability should come naturally to the casual reader. Recall the dynamicist's lament that a nadir-oriented tether (along the local vertical) will not develop a radial acceleration component of the Lorentz force. Librations in the tether provide a non-zero cross product of the tether current and the B field as the tether subject to librations is no longer aligned with the local vertical. Williams' analysis shows a 1.5% improvement in orbit boost using the tether with librations model.

Following the assumption that satellite orbit motion can be manipulated via electrodynamic tether-applied low thrust accelerations, the real constraint shifts from the traditional limitation of onboard propellant storage to one of magnetic field availability in conjunction with current producing power capability. Under this supposition, any spacecraft capable of generating sufficient current to implement Lorentz force-generated acceleration could ostensibly manipulate orbital parameters in any desired fashion. While not a "free lunch" for maneuvering, the prospects of long term maneuvering capability with significantly less propellant mass fraction are appealing and worthy of further study. Electrodynamic tether research in recent years has steadily increased. This field of study is ready for continued effort towards development of on orbit testing. A worthwhile precursor to program development is a review of electrodynamic tether history.

III. ELECTRODYNAMIC TETHER HISTORY

A. GEMINI

Although conceptualized at the beginning of the twentieth century, in ideas such as the “space tower”, it was not until the late 1960’s that space tethers became a reality. Gemini missions 11 and 12 both incorporated a space tether. The tether provided astronauts with a milligee (.001g) of local acceleration which helped with orientation. These astronauts also experienced first-hand the dynamic complexities of the tether.

Figure 11. Gemini Crew with Tether

Later, in 1974, Italian Giuseppe Colombo theorized that a tether between two orbital objects could produce power. He actively pursued his theory, which was realized in the Tethered Satellite Experiment.

B. TETHERED SATELLITE EXPERIMENT (TSS-1)

Launched in July of 1992, it was a joint experiment between Italy and the United States. It consisted of a 518 kg metal sphere with a diameter of 1.6 m that housed ten experiments. The sphere was to be reeled out of the Space Shuttle’s cargo bay. The 22-km tether consisted of 10 34 AWG wire covered in Kevlar, Nomex, and Teflon to create a cable of 2.54 mm diameter. Ideally, the tether would provide enough power to run all

ten experiments aboard to duration. Unfortunately, during the deployment, a protruding bolt on the winch limited deployment to 840 ft, a mere 1% of planned length. Figure 12 (courtesy NASA / NSSDC Master Catalog[17,18]) shows the TSS spacecraft.

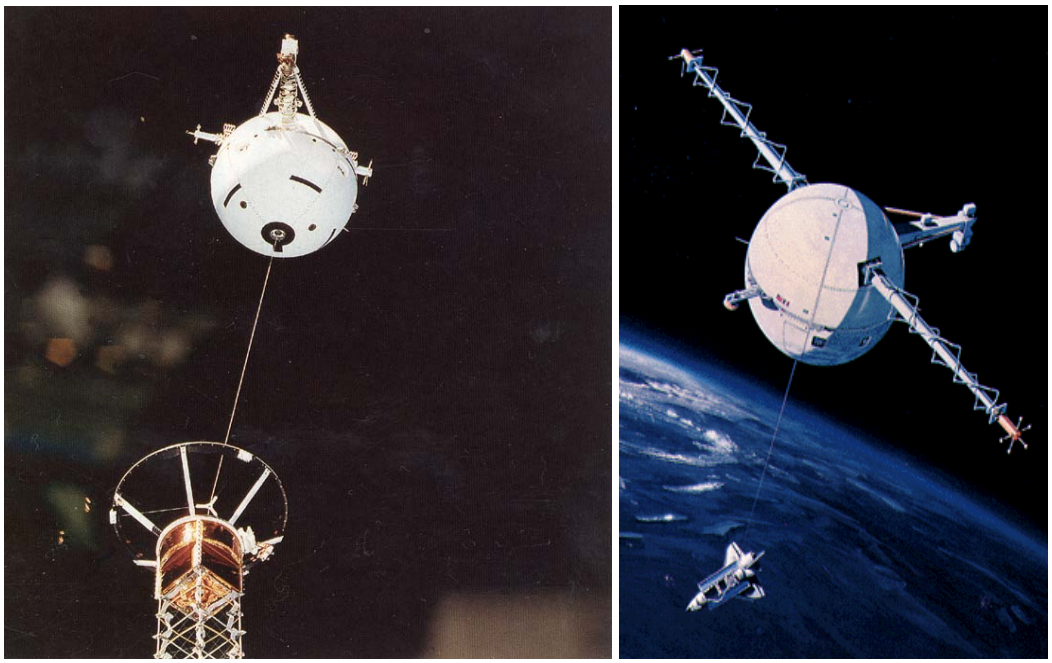

Figure 12. TSS file photography and TSS-1R artist rendition (from Refs. 15,16)

C. TETHERED SATELLITE EXPERIMENT REFLIGHT (TSS-1R)

TSS-1R was launched in February 1996. Approximately five hours after deployment, with 19.7 km (of 20.7 km planned) deployed, the tether snapped near the top of the deployment boom. A peak current of 1.1A was collected; power in excess of 2 kW was generated.[19]

[17] Becky Bray and Patrick Meyer, editors. "Liftoff to Space Exploration," archived website hosted by National Aeronautics and Space Administration, website accessed 10 Feb 2006. http://liftoff.msfc.nasa.gov/shuttle/sts-75/tss-1r/tss-1r.html.

[18] Dr. Frank Six, National Space Science Data Center, National Aeronautics and Space Administration, Marshall Space Flight Center, Huntsville, AL, Master Catalog display website updated 09 Nov 2005, accessed 10 Feb 2006. http://nssdc.gsfc.nasa.gov/database/MasterCatalog?sc=TSS-1.

[19] L. Johnson. "The Tether Solution," *IEEE Spectrum*, Vol. 37, No. 7, pp. 41-42.

D. SMALL EXPENDABLE DEPLOYMENT SYSTEM (SEDS)

Both SEDS operations were launched as secondary payloads aboard Delta rockets on USAF missions. SEDS 1 was launched from Cape Canaveral in March 1993. The main purpose was to demonstrate the viability of space tether deployment and stabilization. A 26-kg mass was ejected by a spring-loaded Marman clamp from the second stage of a Delta rocket. It was released with an initial velocity of 1.6 m/s. This was adequate for the mass to clear the second stage and allow gravity gradient effects to orient the two masses in a local vertical. The tether unwound successfully using both passive and active braking to gently bring the mass to a stop without snapping the tether. After one orbit, the tether was cut by micrometeoroid debris. Despite its premature ending, the mission was successful in demonstrating deployment techniques.

SEDS 2 was launched in March 1994. Mission success required tether deployment of at least 18 km with a residual swing angle of less than 15 degrees. All 19.7 km were deployed with a swing angle of less than four degrees. The tether remained intact for almost four days, before suffering the same fate as its predecessor. After separation, the lower mass re-entered the atmosphere, but the upper mass remained in orbit with the remainder of the tether maintaining a nearly vertical configuration. This was a surprise as the calculated effective end mass of the tether was less than four grams.

E. PLASMA MOTOR GENERATOR (PMG)

NASA's PMG launched aboard a USAF Delta in June 1993. As the name implied, this satellite's purpose was to display the validity of tether power generation and thrust. The satellite deployed a 500 m electrodynamic tether. Marshall Space Flight Center declared the mission a success. The satellite successfully converted orbital energy into electrical energy (de-orbiting) and vice-versa (orbit raising)[20,21] . It showed that magnetic propulsion is effective for short durations around planets with magnetic fields and ionospheres. Of note, this experiment is a milestone for interplanetary

[20] L. Johnson, "The Tether Solution," *IEEE Spectrum*, Vol. 37, No. 7, pp. 41-42.

[21] M. D. Grossi and E. McCoy, "What Has Been Learned in Tether Electrodynamics from the Plasma Motor Generator (PMG) Mission on June 1993," ESA/International Round Table on Tethers in Space, ESTEC Conference Centre, Noordwikj, The Netherlands, 28-30 September 1994.

electrodynamic tether programs, particularly in the case of tether-induced propulsion around Jupiter, where the sizeable magnetic field would prove exceptionally useful.[22]

F. TETHER PHYSICS AND SURVIVABILITY EXPERIMENT (TIPS)

A Naval Research Laboratory experiment, TiPS was launched aboard a Delta rocket in May 1996 to study the long-term effects of space on tethers. The two masses (53 kg each) were separated by a four kilometer wire. The two masses were named for famous Honeymooners' characters Ralph and Norton (Figure 13 below). Norton carried no electronics and was the electron sump. Ralph carried all the instrumentation. Designed to demonstrate tether longevity, the mission surprisingly lasted in excess of three years to 2000 and revealed many characteristics of tethers on orbit. It showed that librations were strongly damped by internal friction over long durations and helped reveal some aspects of tether susceptibility to micrometeoroid impacts. Overall, the experiment exceeded scientists' expectations: the Harvard Smithsonian Center for Astrophysics reported that TiPS proved "a sufficiently fat tether can survive for a very long time."[23]

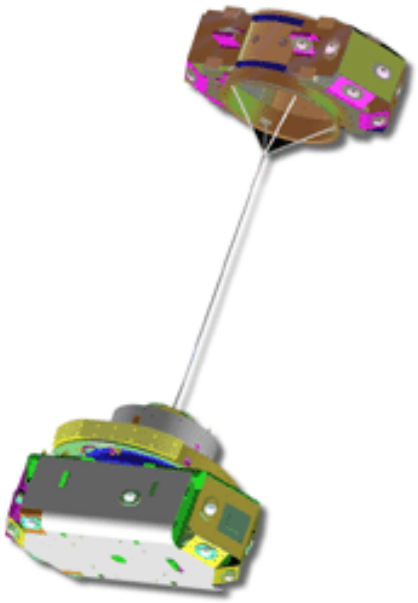

Figure 13. Ralph and Norton of TiPS

[22] E. Lorenzini and Juan Sanmartin, "Electrodynamic Tethers in Space," *Scientific American*, August 2004.

[23] Harvard-Smithsonian Center for Astrophysics. Cambridge, MA, website accessed 10 February 2006: http://cfa-www.harvard.edu/~spgroup/missions.html.

G. PROPULSIVE SMALL EXPENDABLE DEPLOYER SYSTEM (PROSEDS)

PROSEDS was to attempt to increase efficiency in electron collection by using a naked metallic tether instead of an insulated wire: the tether itself was designed to collect electrons rather than through the use of a hollow cathode. The design was to average current over 1 Amp, to a peak of 5 Amps. This would generate an average power of 1.46 kW, and could produce an average thrust of 1N[24]. The design ultimately was to demonstrate the deorbit capability of the tether system, using the Delta II upper stage as the test case. Though this mode of electron collection was thought to be significantly more efficient than previous experiments, the 2000 launch was delayed until as late as June 2003 when hopes were set to ride a GPS mission as a secondary payload. The launch was cancelled by October 2003.

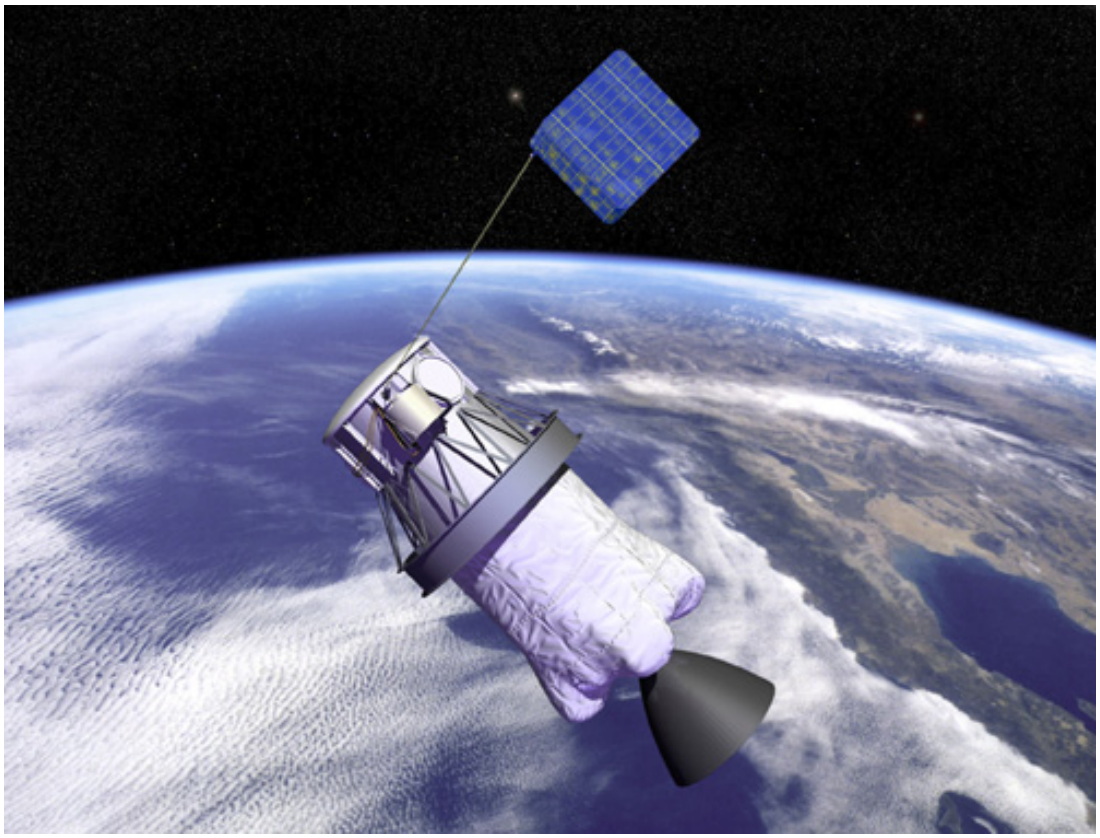

Figure 14. NASA artist rendering of PROSEDS mission (from Ref .20)[25]

[24] L. Johnson. "The Tether Solution," *IEEE Spectrum*, Vol. 37, No. 7, July 2000. National Aeronautics and Space Administration. pp. 42.

[25] Dr. Anthony R. Curtis. "Space Today Online," Laurinburg, NC, http://www.spacetoday.org/images/Rockets/FutureSpaceVehicles/SailProSEDS.jpg, accessed 10 Feb 2006.

H. RECENT RESEARCH

Promising launches aside, no further effort towards on orbit testing of electrodynamic tethers has been considered. This is by no means an indication of a stagnant research field. On the contrary, notable scientific journals have consistently featured tether related work. In fact, a cursory literature review found over 100 refereed journal articles and technical reports on electrodynamic tethers. A comprehensive bibliography of reports from 1971 through 1999 is available from the Harvard Smithsonian Center for Astrophysics and is not repeated here; however a summary of recent research is provided, as the most current developments became motivators for this thesis.

Cited in earlier chapters, Hoyt's work on stabilization of tethers discusses dynamic equilibrium and feedback control usage with librating tethers under perturbing forces. Pelaez and Andres[26] and Somenzi, et al[27], also address tether stability in specific circumstances, demonstrating periodic solutions to governing equations and electrodynamic force coupling of tether oscillations, respectively. Mankala and Agrawal[28] introduce a "variable resistor in series with the tether as a control parameter" for equilibrium to equilibrium motion. Further recommendations for control actuation of tethers are provided in Williams, et al.[29] Lanoix, et. al.[30], presented a model of the tethered system for long term analysis of the Lorentz force effects and developed a control methodology for librations in a deorbit scenario. The guidance control

---

[26] J. Pelaez and Y. N. Andres, "Dynamic Stability of Electrodynamic Tethers in Inclined Elliptical Orbits," *Journal of Guidance, Control, and Dynamics*, Vol. 28, No. 4, July-August 2005. American Institute of Aeronautics and Astronautics.

[27] L. Somenzi, L. Iess, and J. Pelaez, "Linear Stability Analysis of Electrodynamic Tethers," *Journal of Guidance, Control, and Dynamics*, Vol. 28, No. 5, September-October 2005. American Institute of Aeronautics and Astronautics.

[28] Kalyan Mankala and Sunil K. Agrawal, "Equilibrium-to-Equilibrium Maneuvers of Rigid Electrodynamic Tethers," *Journal of Guidance, Control, and Dynamics*, Vol. 28, No. 3, May-June 2005. American Institute of Aeronautics and Astronautics.

[29] Paul Williams, Takeo Watanbe, Chris Blanksby, Pavel Trivailo, and Hironori A. Fujii, "Libration Control of Flexible Tethers Using Electromagnetic Forces and Movable Attachment," *Journal of Guidance, Control, and Dynamics*, Vol. 27, No. 5, September-October 2004. American Institute of Aeronautics and Astronautics.

[30] Eric L. M. Lanoix, Arun K. Misra, Vinod J. Modi, and George Tyc. "Effect of Electrodynamic Forces on the Orbital Dynamics of Tethered Satellites". *Journal of Guidance, Control, and Dynamics*, Vol. 28, No. 6, November-December 2005.

methodology developed by Tragresser and San[31] marks a significant push towards control development for orbital maneuvering. Williams' addition of tether libration dynamics to the Tragresser and San model increased simulation fidelity.

[31] S. G. Tragresser and Hakan San, "Orbital Maneuvering with Electrodynamic Tethers," *Journal of Guidance, Control, and Dynamics*, Vol. 26, No. 5, 2003. American Institute of Aeronautics and Astronautics.

THIS PAGE INTENTIONALLY LEFT BLANK

IV. OPTIMAL ORBIT MANEUVERS

A. PROBLEM FORMULATION: PROBLEM (T)

The specific objective of this section of the thesis is to present one variation in the set of optimal orbit transfer problems. The problem formulation will be constructed for usage with the dynamic optimization program DIDO, with expectation for follow-on work including subsequent problem formulations of other orbit transfer variations. Our particular variation of choice is to search for the optimal control current required to implement a minimum time orbit transfer within a LEO orbit. A typical optical payload satellite specific application of this minimum time orbit transfer resides in any satellite servicing operational concept. We designate this formulation as Problem (T). Following problem formulation and dynamic model validation, the totality of necessary conditions for optimality is evaluated. Conclusions and recommendations for future work complete this chapter.

1. State Vector

The state vector is chosen to be the six classical orbital elements, which completely describe a unique orbit; equinoctial elements are not employed but left for future iterations of the formulation. It follows then that the state vector is:

$$\underline{x}^{T} = \left[a, e, i, \Omega, \omega, \nu \right]$$

Boundaries for the state vector elements follow in table 3. Note eccentricity is limited to values greater than 0 and less than 1 in order to eliminate singularities associated with circular and parabolic orbits, respectively. Likewise, inclination is restricted to positive angles to avoid a singularity in trigonometric relationships resident in the dynamic system equations. True anomaly and problem time are inextricably linked, in that each LEO period takes a corresponding amount of time units to complete. Therefore, true anomaly (the sixth state variable) is arbitrarily set to a high number to allow optimization routines freedom to minimize orbit transfer time without an accidental state boundary.

Variable	Nomenclature	Lower Bound	Upper Bound
a	Semimajor Axis	R_e	3* R_e
e	Eccentricity	0.001	.999
i	Inclination	0.001^o	90^o
Ω	Right Ascension of Ascending Node	0^o	360^o
ω	Argument of Perigee	0^o	360^o
ν	True Anomaly	0^o	360^o x 2000

Table 3. State Vector Lower and Upper Bounds

The significant parametric relationships to other variables are repeated here for ease of reference, specifically the semi-parameter *p*, the orbital angular momentum *h*, and the orbit radius *r*. During problem formulation the importance of these parameters was not underemphasized since each parameter carries information significant to understanding the orbit state during transient periods in the maneuver. Follow on work, such as the transformation of this state vector from classical orbital elements to the equinoctial set of elements, will make use of these expressions in the transformation.

$$p = a(1-e^2)$$
$$h = \sqrt{\mu p}$$
$$r = p/(1+e\cos(\nu))$$

2. Control

The control variable is established as the tether current, I, in amperes, and is limited to 4 amperes. Following the perturbative accelerations used by both Williams[32] and Tragresser and San[33], a control in R^3 could have been employed using the three

[32] Paul Williams. "Optimal Orbit Transfer with Electrodynamic Tether,: *Journal of Guidance, Control, and Dynamics* Vol. 28, No. 5. 2005 American Institute of Aeronautics and Astronautics.

[33] Steven G. Tragresser and Hakan San, "Orbital Maneuvering with Electrodynamic Tethers," *Journal of Guidance, Control, and Dynamics*, Vol. 26, No. 5, 2003.

directions of perturbative force. In this case, however, the singly applied current was chosen to focus the optimization on the one real world controllable parameter, current. The control is box constrained between positive and negative 4 amperes and can be described as:

$$\underline{\mathrm{u}} = \left[I \right] \; ; \; \mathrm{U} = \left\{ (u) : \;\; u \le \left| 4 \right| \right\}$$

3. Dynamics

Using the control current interaction with the Earth magnetic field (B field), the perturbative accelerations are the primary driver for dynamic change of the state variables. Following the flow of expressions begins with the representation of the Earth magnetic field as described in Chapter II. The subscripts are the I, J, and K directions of each B field component respectively. The constant μ_m is the product of the dipole magnetic moment of the Earth and the permeability constant, units are Tesla-m^3. It follows that the units of each B field component are Tesla.

$$B_I = -2(\mu_m / \mathrm{R}^3)\sin(\omega + \nu)\sin(i)$$
$$B_J = (\mu_m / \mathrm{R}^3)\cos(\omega + \nu)\sin(i)$$
$$B_K = (\mu_m / \mathrm{R}^3)\cos(i)$$

Once the B field terms are determined, the perturbative accelerations that affect satellite motion can be calculated following the expressions listed on the next page. Note the first term on the right side of the equations is the control current I. Given the B field units are Tesla (T = kg/(As^2), unit analysis of the expressions shows units on the right hand side of the equation as Amp*meter / kg * (kg /(As^2), which reduces to m/s^2, standard units for acceleration. The *r*, θ, and *h* subscripts indicate the radial, tangential, and orbit normal directions respectively. Recall from the introductory notes that tether librations are described in two dimensions, θ and ϕ. These angles factor into the perturbation accelerations via trigonometric relationships to the three-axis system. By

inspection the expressions hold for stated kinematics in that for a non-librating tether (i.e. θ=ϕ=0) the radial acceleration component f_r is zero.

$$f_r = IL/m(B_z \sin(\theta)\cos(\phi) - B_y \sin(\phi))$$
$$f_\theta = IL/m(B_x \sin(\phi) - B_z \cos(\theta)\cos(\phi))$$
$$f_h = IL/m(B_y \cos(\theta)\cos(\phi) - B_x \sin(\theta)\cos(\phi))$$

Indeed, for a non-librating tether the above perturbation acceleration expressions reduce to:

$$f_r = 0$$
$$f_\theta = -IL/m(B_z)$$
$$f_h = IL/m(B_y)$$

The perturbative acceleration terms are then employed in the Gauss form of the variational equations[34],[35]

$$\dot{a} = (2a^2/h)[e\sin(\nu) f_r + (p/r) f_\theta]$$
$$\dot{e} = (1/h)\{p\sin(\nu) f_r + [(p+r)\cos(\nu) + re] f_\theta\}$$
$$\dot{i} = (r\cos(\omega+\nu)/h) f_h$$
$$\dot{\Omega} = (r\sin(\omega+\nu)/h\sin(i)) f_h$$
$$\dot{\omega} = (1/he)[-p\cos(\nu) f_r + (p+r)\sin(\nu) f_\theta]$$
$$-[r\sin(\omega+\nu)\cos(i)/h\sin(i)] f_h$$
$$\dot{\nu} = h/r^2 + [(1/eh)[p\cos(\nu) f_r - (p+r)\sin(\nu) f_\theta]$$

Kechichian presents a state vector with the last element as Mean anomaly vice true anomaly as represented here, and further recommends transformation to the

34 Paul Williams. "Optimal Orbit Transfer with Electrodynamic Tether,: *Journal of Guidance, Control, and Dynamics* Vol. 28, No. 5. 2005 American Institute of Aeronautics and Astronautics.

35 J.A. Kechichian, "Trajectory Optimization Using Nonsingular Orbital Elements and True Longitude," *Journal of Guidance, Control, and Dynamics* Vol. 20, No. 5. 1997. American Institute of Aeronautics and Astronautics.

equinoctial set of elements[36]; Mendy[37] also presents a valuable discussion of the merits of the equinoctial set. This thesis formulation maintained the variational equations with simpler classical orbital elements as used by both Williams and Tragresser and San, leaving state vector transformation to the equinoctial set of elements for future work.

It is noted that the electromagnetic torques provided by the current-carrying tether in the magnetic field have models that are available for inclusion; however, these torques were not employed in this formulation as the perturbative accelerations contain all the necessary information to relate applied control to the first order state vector dynamics equations. The tether librations are described by second order differential equations which are omitted from initial formulations for simplicity. Simplification of this nature merely implies a tether rigidly aligned to the local vertical (nadir pointing) so that libration angles θ and ϕ are zero. The tethered satellite state and control representation complete, it is observed that Problem (T) defines $x \in \mathrm{R}^6$ and $u \subset \mathrm{U} \in \mathrm{R}$. The next step is to define the cost function and events file for optimization.

4. Cost

As Problem (T) seeks to *minimize* the time required to transfer from one initial orbit to a final orbit, the primary cost function used is a Mayer cost set to value of final time, t_f. A Lagrange cost function F= (u^2) can be considered in order to develop a Bolza cost function to minimize control power required but is not used in the standard formulation and is left for follow-on work. The cost function as presented is then $J[x(\cdot), u(\cdot), t_f] = t_f$.

5. Events

Initial parameters are given as:

---

[36] J.A. Kechichian, "Trajectory Optimization Using Nonsingular Orbital Elements and True Longitude," *Journal of Guidance, Control, and Dynamics* Vol. 20, No. 5. 1997. American Institute of Aeronautics and Astronautics.

[37] Paul B. Mendy, Maj., USAF, "Multiple Satellite Trajectory Optimization," Naval Postgraduate School Thesis, December 2004.

$$(\mathrm{a}_0,\ \mathrm{e}_0,\ \mathrm{i}_0,\ \Omega_0, \omega_0, \nu_0)\ =\ (6717km, 0.02, 51.59^o, 0^o, 50^o, 0^o),$$

which comprise the orbital element set at problem start.

Endpoint conditions are $(\mathrm{a}_f, \mathrm{e}_f,\ \mathrm{i}_f) = (7217km, 0.02, 51.59^o)$.

The final values for Right ascension of the ascending node, argument of perigee, and true anomaly are free from endpoint constraints as these elements of the satellite state vector in orbit are not considered important. Future iterations of this problem formulation will add constraints for the remaining state variables. Note the final values for eccentricity and inclination are equal to the initial values: essentially the events shape Problem (T) to be a minimum time, orbit raising problem with no requirement for orbit phasing. The endpoint function is $\bar{E}(a_f, e_f, i_f) = E + \nu^T \underline{e}$, more fully represented as:

$$\bar{E}(a_f, e_f, i_f) = t_f + \begin{bmatrix} \nu_a \\ \nu_e \\ \nu_i \end{bmatrix}^T \begin{bmatrix} a_f - 7217 \\ e_f - 0.02 \\ i_f - 51.59^\circ \end{bmatrix}$$

where

$$E(\underline{x}_f, t_f) = t_f \text{ and } e(\underline{x}_f, t_f) = \underline{e}_f - \underline{e}^f .$$

Taking into account all the earlier relationships, the final problem formulation is fully stated as follows:

$$
\text{Problem(T)}\begin{cases}
\text{Minimize } J[\mathrm{x}(\cdot),\, \mathrm{u}(\cdot),\, t_f] = t_f \\
\text{Subject to} \quad \dot{\mathrm{a}} = (2a^2/h)[e\sin(\nu) f_r + (p/r) f_\theta] \\
\qquad\qquad \dot{\mathrm{e}} = (1/h)\{p\sin(\nu) f_r + [(p+r)\cos(\nu) + re] f_\theta\} \\
\qquad\qquad \dot{\mathrm{i}} = (r\cos(\omega+\nu)/h) f_h \\
\qquad\qquad \dot{\Omega} = (r\sin(\omega+\nu)/h\sin(i)) f_h \\
\qquad\qquad \dot{\omega} = (1/he)[-p\cos(\nu) f_r + (p+r)\sin(\nu) f_\theta] \\
\qquad\qquad\qquad\qquad -[r\sin(\omega+\nu)\cos(i)/h\sin(i)] f_h \\
\qquad\qquad \dot{\nu} = h/r^2 + [(1/eh)[p\cos(\nu) f_r - (p+r)\sin(\nu) f_\theta] \\
(a_0,\, e_0,\, i_0,\, \Omega_0, \omega_0, \nu_0) \;=\; (6717km, 0.02, 51.59^o, 0^o, 50^o, 0^o) \\
\qquad (a_f, e_f,\, i_f) \;=\; (7217km, 0.02, 51.59^o)
\end{cases}
$$

B. SCALING AND BALANCING: PROBLEM (T)

Equipped with a satisfactory problem definition, it is necessary to establish scaling and balancing of the dynamic relationships for numerical computation efficiency. A preliminary planning method is to consider the operating range of values for each parameter involved in problem formulation. This allows for easy recognition of possible computation irregularities brought about by large scale differences in numeric quantities.

Parameter	**Nomenclature**	**Range (MKS units)**	**Order**
x_1	Semimajor Axis	[6378000 7217300] meters	10^6
x_2	Eccentricity	[0 1] (dimensionless)	10^0
x_3, x_4, x_5	Inclination, Argument of Perigee, RAAN	[0 2π] radians	10^0
x_6	True Anomaly	[0 100] radians	10^2
u	Current (control)	[-4 4] amperes	10^0
M	Mass	[450] kg	10^2

Table 4. Relative Order of Magnitude for Problem Parameters

As is apparent from Table 4, there is a large discrepancy in the order of magnitude of state variables, particularly with respect to the state variable x_1 compared to the small quantities expected in other parameters. Eccentricity (x_2) is defined between 0 and 1 for an elliptical orbit and does not require scaling. Likewise, scaling is not desired for radian measurements in the case of the latter four state variables (Inclination, RAAN, Argument of perigee, and True Anomaly). Mass and Length scaling factors were chosen to achieve unity for mass and final semimajor axis values. In order to also scale the control parameter of current to +/- unity, the time unit was adjusted following MKS definitions for the Ampere (kg-m^2/s^4), so that one time unit = $\sqrt[4]{MassU \cdot Du^2 / Amp}$. This achieves balancing of the dynamic equations in addition to scaling the final time guess (tfGuess) from 100000 seconds to 17.144 Time units (Tu). A summary of scaling efforts is contained in Table 5 on the following page.

Principal Parameters					
Parameter	**Metric Unit**	**Value (if const)**	**Scaling**		
			Factor	**Application**	**Value**
Mass	Kilogram	450	$MassU$ = m	$\bar{m} = m / MassU$	1
Length	Meter	af= 7217326.3	Du = a_f	$\bar{a} = a / Du$	1
Time	Second	t_f Guess =100000	$Tu = \sqrt[4]{MassU \cdot Du^2 / Amp}$ = 8749.360	$\bar{t} = t / Tu$ =100000/8749.360	17.144
Other parameters / constants					
Current	$Amps = kg\ m^2 / s^4$	*4*	$\bar{I} = I \frac{Tu^4}{(MassU \cdot Du^2)}$	*4*8749^4 (450*7217326.3^2)*	1
μ_g	$\frac{m^3}{s^2}$	*3.9860044 x 10^{14}*	$\bar{\mu}_g = \frac{\mu_g}{(Du^3 / Tu^2)}$	*3.98e14 7217326.3^3/8749 ^2*	81.164
μ_m	$\frac{kg\ m^3}{As^2}$	*1.0179 x10^{17}*	$\bar{\mu}_m = \mu_m \cdot \frac{Scale.amps \cdot Tu^2}{(MassU \cdot Du^3)}$	*4*8749^2 450*7217326^3*	184.23

Table 5. Scaling and Balancing Relationships

The newly scaled parameters now have the ranges displayed below in Table 6.

Parameter	Nomenclature	Range (Scaled units)	Order
x_1	Semimajor Axis	[.9 1.5] Distance Units	10^0
x_2	Eccentricity	[0 1] (dimensionless)	10^0
x_3, x_4, x_5	Inclination, Argument of Perigee, RAAN	[0 2π] radians	10^0
x_6	True Anomaly	[0 2πn] radians (n=#orbits)	10^2
u	Current (control)	[-1 1] Amp Units	10^0
M	Mass	[1] Mass Units	10^0
T	Time	[0 10.7] Time Units	10^0

Table 6. Scaled Problem Parameters

C. ANALYSIS: PROBLEM (T)

The following subsections detail the computational optimization work. Analysis was performed using DIDO 2003e on MATLAB Version 6.5. For initial problem runs, 30 nodes were employed. Given a locally optimal solution from DIDO, states were reused as guess values for a 90-node problem run. This process of bootstrapping the solution from 30 to 90 nodes was used to establish the results for all following analysis.

1. Feasibility

Physical expressions were first evaluated by unit analysis to ensure parameters were in correct physical units. Feasibility is further assessed via MATLAB ode45 propagation of the controls. Following a successful (no infeasibilities) DIDO run, *primal.controls* is sent to a propagator function where the data is interpolated using a spline method. The resulting optimal control $\underline{u}^*$ is propagated through the dynamics equations to determine the resultant state vector. This output is plotted over *primal.states*, the optimal state solution. Visual concurrence between DIDO output (plotted as red circles at each node) and the propagator output (a blue line) was achieved. Numerical concurrence was evaluated by normalized error comparisons for each state at

the last node. Graphical representation of feasibility is displayed in Figures 15 through 20 on the following pages. Of note, true anomaly increases linearly, consistent with low eccentricity orbital motion.

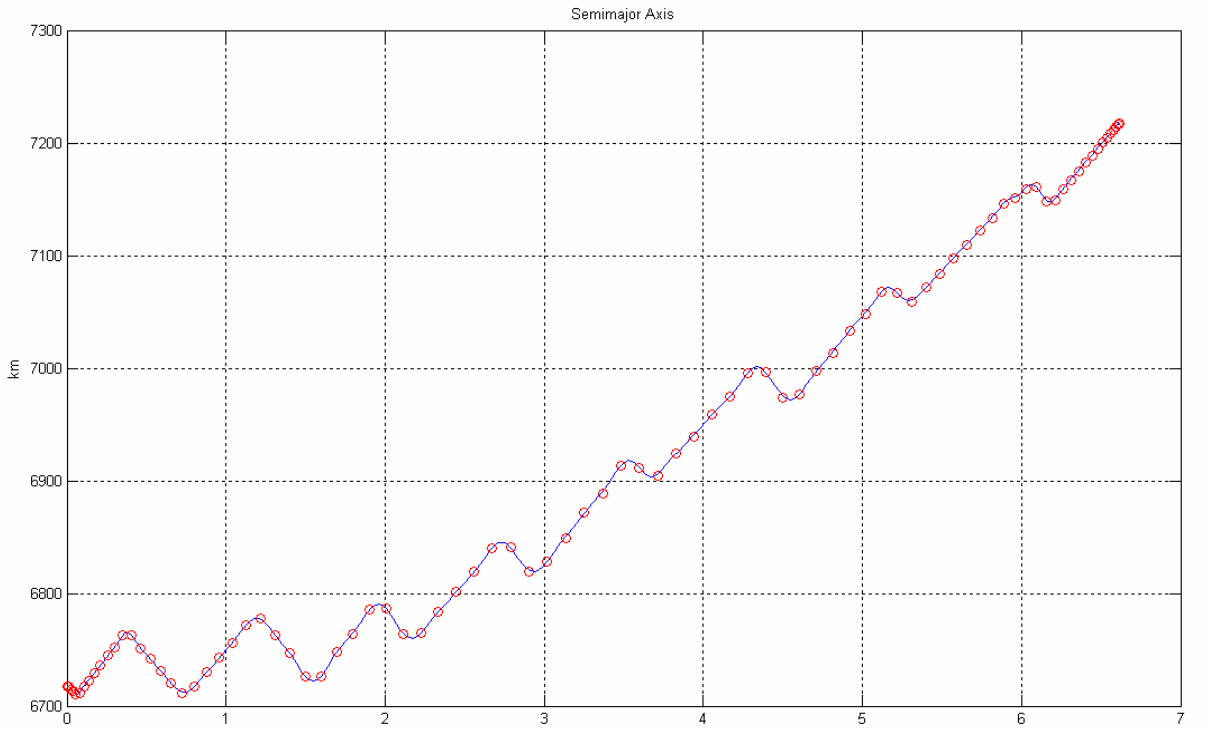

Figure 15. Problem (T): Feasibility demonstrated in semimajor axis (90 nodes employed)

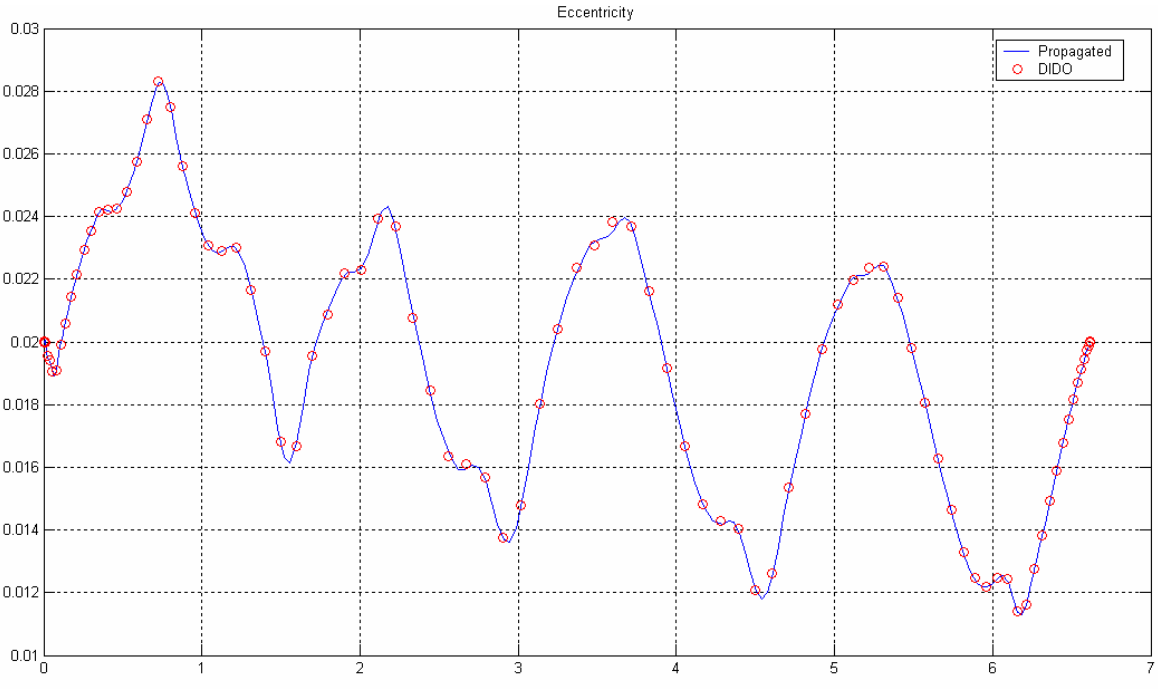

Figure 16. Problem (T): Feasibility demonstrated in Eccentricity (90 nodes employed)

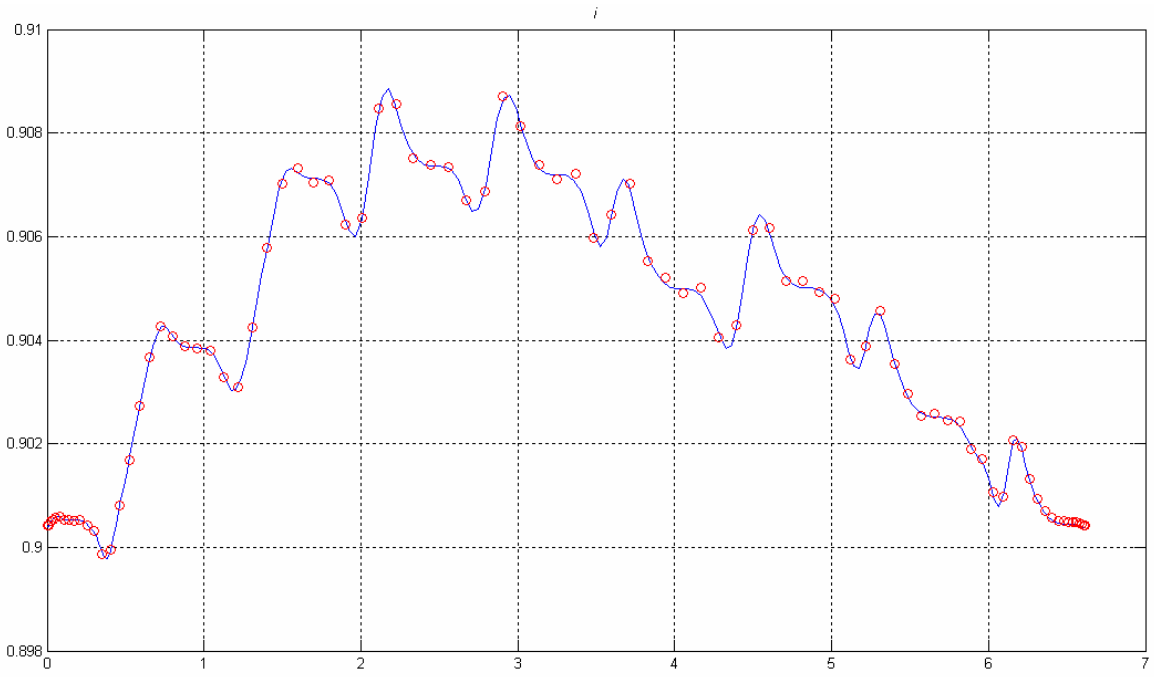

Figure 17. Problem (T): Feasibility demonstrated in Inclination (90 nodes employed)

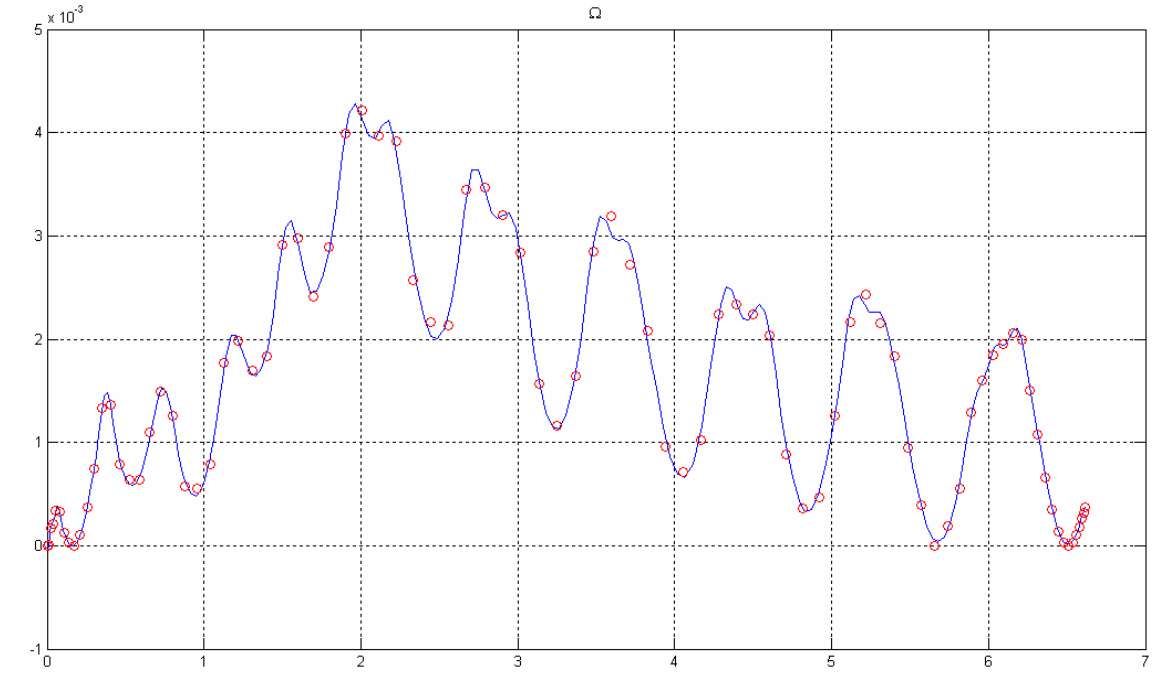

Figure 18. Problem (T): Feasibility demonstrated in Ascension of Ascending Node (90 nodes employed)

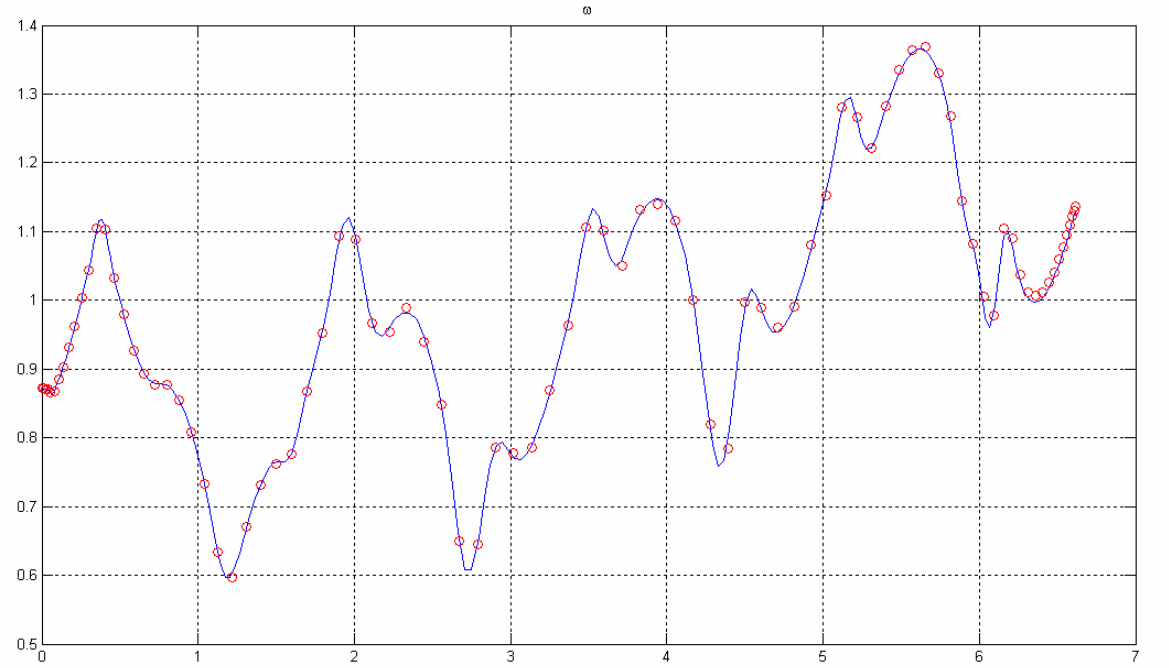

Figure 19. Problem (T): Feasibility demonstrated in Argument of Perigee (90 nodes employed)

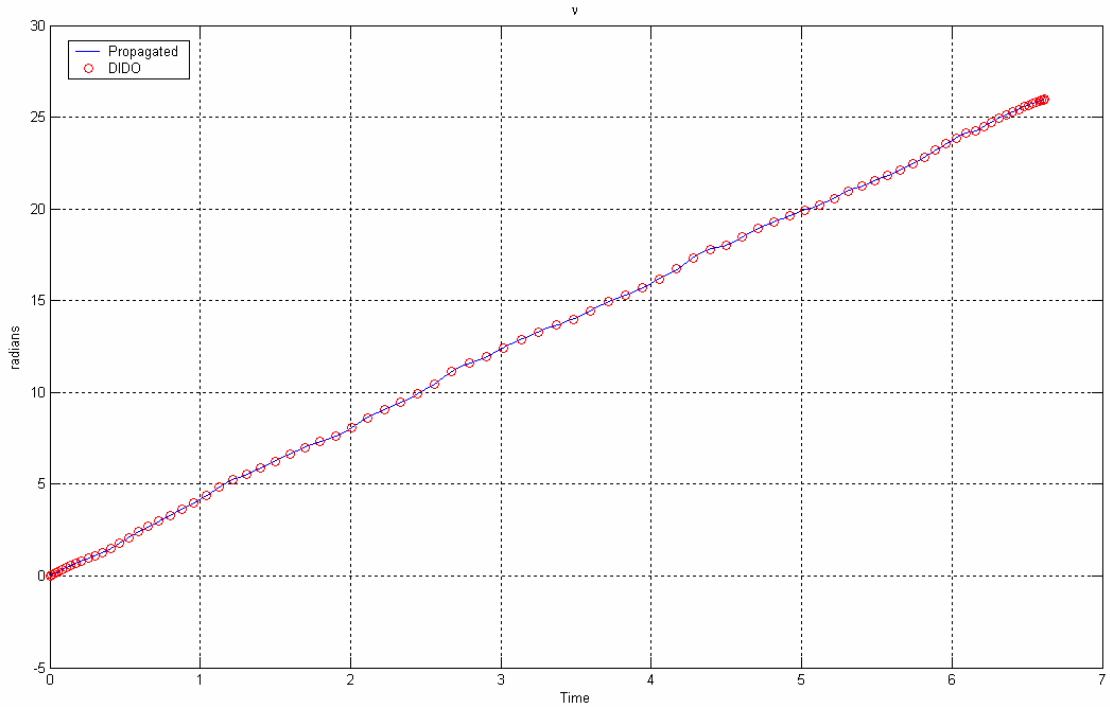

Figure 20. Problem (T): Feasibility demonstrated in true anomaly (90 nodes employed)

The optimal control $\underline{u}^*$ developed is displayed in Figure 21. Note the control versus time plot represents the optimal control as determined using 90 nodes. The number of nodes can be loosely interpreted as a "resolution factor" for discrete solutions attempting to approximate continuous time results, e.g. more nodes = higher resolution. Following this interpretation, it is believed that increasing the number of nodes or revisiting the optimal control solution by starting at a different node would in fact deliver a uniform bang-bang control result. Points in the below plot where "throttled" values other than +/- 4 Amps are seen are possibly the result of chatter in the vicinity of the control affected by the switching function or can be attributed to model resolution.

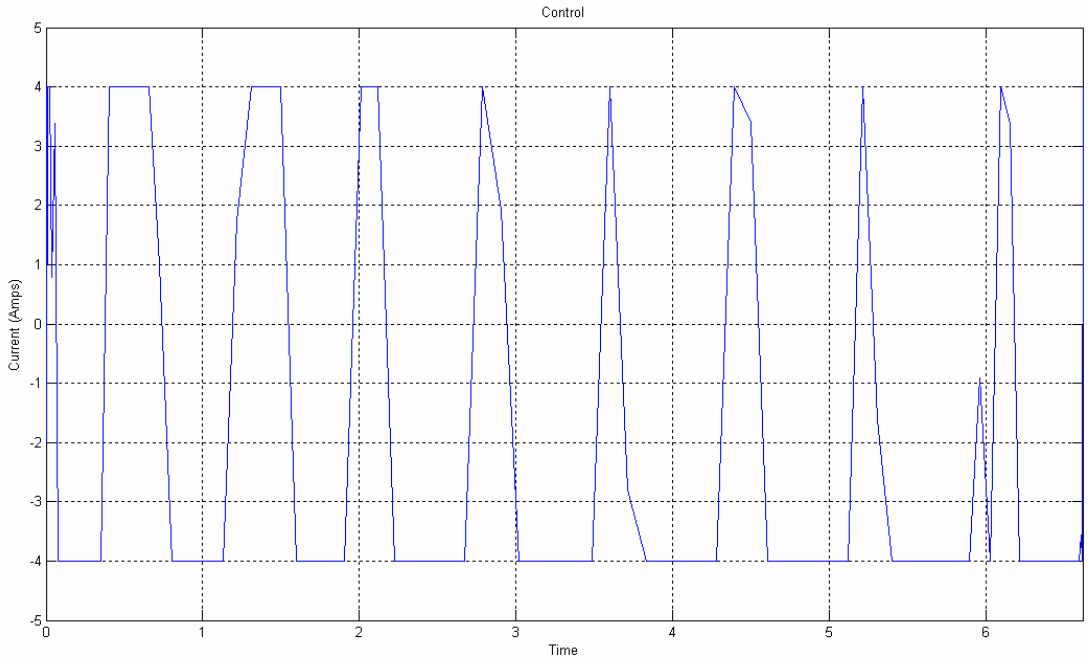

Figure 21. Problem (T): Optimal Control Current applied (90 nodes employed)

Now that feasibility and rational expectations of the solution are met, it is appropriate to consider the optimality of the results.

2. Optimality

The totality of optimality conditions was assessed. The Hamiltonian was first constructed following[38]: $H(\boldsymbol{\lambda}, \mathbf{x}, \mathbf{u}, t) = F(\mathbf{x}, \mathbf{u}, t) + \boldsymbol{\lambda}^T f(\mathbf{x}, \mathbf{u}, t)$,

where the costate vector $\boldsymbol{\lambda} = [\lambda_a \lambda_e \lambda_i \lambda_\Omega \lambda_\omega \lambda_\nu] = [\lambda_{x_1} \lambda_{x_2} \lambda_{x_3} \lambda_{x_4} \lambda_{x_5} \lambda_{x_6}]$. As stated in paragraph A4 of this chapter, there is no "running" cost associated with this particular problem formulation: $F(\mathbf{x}, \mathbf{u}, t) = 0$. The Hamiltonian expression reduces to $H(\boldsymbol{\lambda}, \mathbf{x}, \mathbf{u}, t) = \boldsymbol{\lambda}^T f(\mathbf{x}, \mathbf{u}, t)$ and is formed by summing the products of each costate multiplier with its respective dynamics function (the right hand side of the first order state vector representation).

$$
\begin{aligned}
H = & \\
& \lambda_a \left[\frac{2a^2}{h} \right] \left[e \sin(\nu) \cdot f_r + (\frac{p}{r}) \cdot f_\theta \right] + \\
& \lambda_e \left[\frac{1}{h} \right] \left[p \sin(\nu) \cdot f_r + \left([p + r] \cos(\nu) + re \right) f_\theta \right] + \\
& \lambda_i \left[r \cdot \frac{\cos(\omega + \nu)}{h} \right] \cdot f_h + \\
& \lambda_\Omega \left[r \cdot \frac{\sin(\omega + \nu)}{h \sin(i)} \right] \cdot f_h + \\
& \lambda_\omega \left[\frac{1}{he} \left[-p \cos(\nu) f_r + [p + r] \sin(\nu) f_\theta \right] - \left[\frac{r \sin(\omega + \nu) \cos(i)}{h \sin(i)} \right] f_h \right] + \\
& \lambda_\nu \left[\frac{h}{r^2} + \left[\frac{1}{eh} \right] \left[p \cos(\nu) f_r - [p + r] \sin(\nu) f_\theta \right] \right]
\end{aligned}
$$

Recall the control definition set forth earlier in this chapter. The constraint upon the applied tether current places the control variable between -4 and 4 amperes (unscaled value). Due to the existence of a path constraint, in this case the "box constraint" upon *u*, the Karush-Kuhn-Tucker (KKT) theorem must be applied to evaluate optimality. (Recall that these conditions set forth by Pontryagin[39] do not guarantee optimality, but optimality requires that the conditions must be satisfied.) This analysis requires construction of the

[38] I. Michael Ross, "Lecture Notes in Control & Optimization," AE4850, 2004. Naval Postgraduate School, Monterey, CA, pp. 115-116.

[39] Pontryagin's Maximum Principle essentially concludes that optimal solutions have to satisfy several observable conditions as "proof" of their optimality. Ross, I. Michael, "Lecture Notes in Control & Optimization," AE4850, 2004. Naval Postgraduate School, Monterey, CA.

Lagrangian of the Hamiltonian, designated $\bar{H}$, where a Lagrangian multiplier μ_L is used[40]. The specific setup for evaluating KKT conditions is $\frac{\partial \overline{H}}{\partial u} = H(\mathbf{x}(), u(), t) + \mu_L{}^T \mathbf{h}(\mathbf{x}(), u(), t)$ where in this formulation the Lagrangian multiplier μ_L is a scalar due to the control $\underline{u} \subset U$. The non-vector nature of the singular control in this problem formulation provides significant simplicity in augmenting the Hamiltonian. The new representation is as follows: $\frac{\partial \overline{H}}{\partial u} = H(\mathbf{x}(), u(), t) + \mu_L{}^T u$.

The now augmented Hamiltonian is useful for recognition of the switching function applicable to the optimal control. The Lagrangian of the Hamiltonian is used to evaluate the Hamiltonian Minimum Condition, which, when combined with other conditions discussed later, will demonstrate the totality of necessary conditions for optimality: Before proceeding it is worthwhile to reproduce the Lagrangian of the Hamiltonian here using state variable references rather than variable designations, (i.e. x_1 rather than *a*).

[40] Note the subscript "L" for this Lagrangian multiplier, differentiating it from the gravitational parameter μ_g and the magnetic dipole moment μ_m discussed earlier in problem formulation.

$$
\begin{aligned}
\bar{H} = \\
&\lambda_{x_1}\left[\frac{2x_1^{\,2}}{\sqrt{\mu x_1(1-x_2^{\,2})}}\right]\left[x_2\sin(x_6)\cdot f_r(x(\cdot),u)+(1+x_2\cos(x_6))\cdot f_\theta(x(\cdot),u)\right]+\\
&\lambda_{x_2}\left[\frac{1}{\sqrt{\mu x_1(1-x_2^{\,2})}}\right]\left[\begin{array}{l} x_1(1-x_2^{\,2})\sin(x_6)\cdot f_r(x(\cdot),u)+\left(\begin{array}{l}\left[x_1(1-x_2^{\,2})+\dfrac{x_1(1-x_2^{\,2})}{1+x_2\cos(x_6)}\right]\cos(x_6)\\ +\left(\dfrac{x_1(1-x_2^{\,2})}{1+x_2\cos(x_6)}\right)x_2\end{array}\right)f_\theta(x(\cdot),u)\end{array}\right]+\\
&\lambda_{x_3}\left[\frac{x_1(1-x_2^{\,2})}{1+x_2\cos(x_6)}\cdot\frac{\cos(x_5+x_6)}{\sqrt{\mu x_1(1-x_2^{\,2})}}\right]\cdot f_h(x(\cdot),u)+\\
&\lambda_{x_4}\left[\frac{x_1(1-x_2^{\,2})}{1+x_2\cos(x_6)}\cdot\frac{\sin(x_5+x_6)}{\sqrt{\mu x_1(1-x_2^{\,2})\sin(x_3)}}\right]\cdot f_h(x(\cdot),u)+\\
&\lambda_{x_5}\left[\begin{array}{l}\left[\dfrac{1}{\sqrt{\mu x_1(1-x_2^{\,2})}x_2}\right]\left[\begin{array}{l}-x_1(1-x_2^{\,2})\cos(x_6)f_r(x(\cdot),u)+\ldots\\ \left[x_1(1-x_2^{\,2})+\dfrac{x_1(1-x_2^{\,2})}{1+x_2\cos(x_6)}\right]\sin(x_6)f_\theta(x(\cdot),u)\end{array}\right]\cdots\\ -\left[\dfrac{\dfrac{x_1(1-x_2^{\,2})}{1+x_2\cos(x_6)}\sin(x_5+x_6)\cos(x_3)}{\sqrt{\mu x_1(1-x_2^{\,2})}\sin(x_3)}\right]f_h(x(\cdot),u)\end{array}\right]+\\
&\lambda_{x_6}\left[\frac{\sqrt{\mu x_1(1-x_2^{\,2})}}{\left(\dfrac{x_1(1-x_2^{\,2})}{1+x_2\cos(x_6)}\right)^2}+\left[\frac{1}{x_2\sqrt{\mu x_1(1-x_2^{\,2})}}\right]\left[\begin{array}{l}x_1(1-x_2^{\,2})\cos(x_6)f_r(x(\cdot),u)\ldots\\ -\left[x_1(1-x_2^{\,2})+\dfrac{x_1(1-x_2^{\,2})}{1+x_2\cos(x_6)}\right]\sin(x_6)f_\theta(x(\cdot),u)\end{array}\right]\right]+\\
&\mu_L\cdot u
\end{aligned}
$$

To minimize the complexity of the expression, the perturbation acceleration expressions (f_r, f_θ, f_h) are not displayed but rather identified as functions of the state variables and control term. This expression assists in analytically differentiating the Lagrangian of the Hamiltonian with respect to the control in order to determine a candidate for $u^*(\cdot)$, the optimal control.

a Hamiltonian Minimization Condition

In order to evaluate the HMC, where according to Pontryagin's Minimization Principle $\frac{\partial \bar{H}}{\partial u} = 0$, each term of the augmented Hamiltonian not dependent upon *u* is represented by a capital letter in its place, thereby simplifying the overall expression. This simplified Hamiltonian will follow the notation H_r in this thesis, and is reproduced on the next page. To avoid introducing confusion, capital letters already presented or defined in this thesis (H, F, E, etc.) will not be used for Hamiltonian terms in the expression not containing *u*.

$$
\begin{aligned}
&\bar{H}_r = \\
&\lambda_{x_1}\left[A\right]\left[C \cdot f_r(x(\cdot),u) + D \cdot f_\theta(x(\cdot),u)\right] + \\
&\lambda_{x_2}\left[F\right]\left[K \cdot f_r(x(\cdot),u) + \left(L\right) f_\theta(x(\cdot),u)\right] + \\
&\lambda_{x_3}\left[M\right] \cdot f_h(x(\cdot),u) + \\
&\lambda_{x_4}\left[N\right] \cdot f_h(x(\cdot),u) + \\
&\lambda_{x_5}\left[\left[O\right]\left[P \cdot f_r(x(\cdot),u) + R \cdot f_\theta(x(\cdot),u)\right] - \left[S\right] f_h(x(\cdot),u)\right] + \\
&\lambda_{x_6}\left[T + \left[U\right]\left[V \cdot f_r(x(\cdot),u) - W \cdot f_\theta(x(\cdot),u)\right]\right] + \\
&\mu_L \cdot u
\end{aligned}
$$

The reduced Hamiltonian expression is now simpler and manageable for partial differentiation with respect to the control variable *u*. Attention is given to the three perturbation acceleration expressions: f_r, f_θ, f_h. Following superposition principles and the chain rule of differentiation, the partial derivatives of each *f* term with respect to *u* ($\frac{\partial \bar{H}_r}{\partial f_{r,\theta,h}}$) are germane to solving $\frac{\partial \bar{H}_r}{\partial u} = \frac{\partial \bar{H}_r}{\partial f_{r,\theta,h}} \frac{\partial f_{r,\theta,h}}{\partial u} = 0.$

From paragraph A3 of this chapter,

$$
\begin{aligned}
f_r &= uL / m(B_z \sin(\theta)\cos(\phi) - B_y \sin(\phi)) \\
f_\theta &= uL / m(B_x \sin(\phi) - B_z \cos(\theta)\cos(\phi)) \\
f_h &= uL / m(B_y \cos(\theta)\cos(\phi) - B_x \sin(\theta)\cos(\phi))
\end{aligned}
$$

Note that *u* has been substituted for the variable for current (I). The partial differentials of each *f* component with respect to control (*u*) are:

$$\frac{\partial f_r}{\partial u} = L/m(B_z \sin(\theta)\cos(\phi) - B_y \sin(\phi))$$
$$\frac{\partial f_\theta}{\partial u} = L/m(B_x \sin(\phi) - B_z \cos(\theta)\cos(\phi))$$
$$\frac{\partial f_h}{\partial u} = L/m(B_y \cos(\theta)\cos(\phi) - B_x \sin(\theta)\cos(\phi))$$

The above differential expressions are now used in the minimized Hamiltonian below:

$$\frac{\partial \bar{H}_r}{\partial u} =$$
$$\lambda_{x_1} L/m[A]\left[C\cdot(B_z \sin(\theta)\cos(\phi) - B_y \sin(\phi)) + D\cdot(B_x \sin(\phi) - B_z \cos(\theta)\cos(\phi))\right] +$$
$$\lambda_{x_2} L/m[F]\left[G\cdot(B_z \sin(\theta)\cos(\phi) - B_y \sin(\phi)) + (K)(B_x \sin(\phi) - B_z \cos(\theta)\cos(\phi))\right] +$$
$$\lambda_{x_3} L/m[M]\cdot(B_y \cos(\theta)\cos(\phi) - B_x \sin(\theta)\cos(\phi)) +$$
$$\lambda_{x_4} L/m[N]\cdot(B_y \cos(\theta)\cos(\phi) - B_x \sin(\theta)\cos(\phi)) +$$
$$\lambda_{x_5} L/m\begin{bmatrix}[O]\left[P\cdot(B_z \sin(\theta)\cos(\phi) - B_y \sin(\phi)) + R\cdot(B_x \sin(\phi) - B_z \cos(\theta)\cos(\phi))\right]... \\ -[S](B_y \cos(\theta)\cos(\phi) - B_x \sin(\theta)\cos(\phi))\end{bmatrix} +$$
$$\lambda_{x_6} L/m\left[T + [U]\left[V\cdot(B_z \sin(\theta)\cos(\phi) - B_y \sin(\phi)) - W\cdot(B_x \sin(\phi) - B_z \cos(\theta)\cos(\phi))\right]\right] +$$
$$\mu_L$$

which gives us an equation for the switching function, since $\frac{\partial \bar{H}_r}{\partial u} = 0$. Considering the zero libration case where θ and ϕ are zero, the above expression reduces to:

$$\frac{\partial \bar{H}_r}{\partial u} =$$
$$\lambda_{x_1} L/m[A][-DB_z] +$$
$$\lambda_{x_2} L/m[F]\left[(-K)B_z\right] +$$
$$\lambda_{x_3} L/m[M]\cdot(B_y) +$$
$$\lambda_{x_4} L/m[N]\cdot B_y +$$
$$\lambda_{x_5} L/m\left[[O][-RB_z] - S(B_y)\right] +$$
$$\lambda_{x_6} L/m\left[T + [U][-W\cdot(B_z)]\right] +$$
$$\mu_L$$

b. Adjoint Equations

The adjoint equation is given by[41] $-\dot{\underline{\lambda}} = \frac{\partial H}{\partial \underline{x}}$, which contains the costate dynamics and is useful not only for describing costate history but is useful in checking terminal values of costates under transversality conditions and also verification of the Hamiltonian.

c. Hamiltonian Evolution Equation

The minimized Hamiltonian for this problem formulation is expected to be constant with respect to time; a cursory check of the dynamic equations shows no terms explicitly dependent upon time. Following the Hamiltonian Evolution Equation we should find the Hamiltonian constant with respect to time. With the Hamiltonian defined as $H \equiv H(\underline{x}(\cdot), u(\cdot), \underline{\lambda}(\cdot), t)$, differentiating the Hamiltonian with respect to time shows the following:

$$\frac{dH}{dt} = \left(\frac{\partial H}{\partial \underline{x}}\right)\frac{\partial \underline{x}}{\partial t} + \left(\frac{\partial H}{\partial \underline{\lambda}}\right)\frac{\partial \underline{\lambda}}{\partial t} + \left(\frac{\partial H}{\partial u}\right)\frac{\partial u}{\partial t} + \frac{\partial H}{\partial t}$$

or more succinctly,

$$\frac{dH}{dt} = \left(\frac{\partial H}{\partial \underline{x}}\right)\dot{x} + \left(\frac{\partial H}{\partial \underline{\lambda}}\right)\dot{\lambda} + \left(\frac{\partial H}{\partial u}\right)\dot{u} + \frac{\partial H}{\partial t}\,.$$

For optimal control, $u = u^*$, substitute $\left(\frac{\partial H}{\partial u}\right)=0$ following Pontryagin's Minimum Principle, and then substitute the adjoint equation from the preceding paragraph, $-\dot{\underline{\lambda}} = \frac{\partial H}{\partial \underline{x}}$. This leaves us with the following expression

$\frac{dH}{dt} = \left(-\dot{\lambda}\right)\dot{x} + \left(\frac{\partial H}{\partial \underline{\lambda}}\right)\dot{\lambda} + (0)\dot{u} + \frac{\partial H}{\partial t}$. Recall from the definition of the

[41] I. Michael Ross, "Lecture Notes in Control & Optimization," AE4850, 2004. Naval Postgraduate School, Monterey, CA, p. 116.

Hamiltonian that $H = F + \underline{\lambda}^T \underline{\mathrm{f}}$, where $\underline{\mathrm{f}} = \underline{\dot{x}}$, then $\frac{\partial H}{\partial \underline{\lambda}} = \underline{\dot{x}}$, which allows us to conclude that $\frac{dH}{dt} = \frac{\partial H}{\partial t}$. It follows that if the Hamiltonian is not dependent upon time, thus

$$\dot{H} = 0$$

d. Hamiltonian Value Condition

Subsequently, the Hamiltonian Value Condition shows the constant value of the minimized Hamiltonian to be negative one, which is consistent with minimum time problems.

$$H\left[t_f\right] = -\frac{\partial \overline{E}}{\partial t} = -1$$

We can then determine that the Hamiltonian is negative one for all time in the interval considered. In Figure 22, the Hamiltonian is plotted versus time. The two conditions (HEE and HVC) expected for a minimum time problem formulation as presented in Problem (T) are met computationally. It is apparent the computationally developed Hamiltonian is approximately negative one, fluctuations notwithstanding, the DIDO solution does in fact correspond to the theoretical value calculated by hand. Reasons for the fluctuations are not understood.

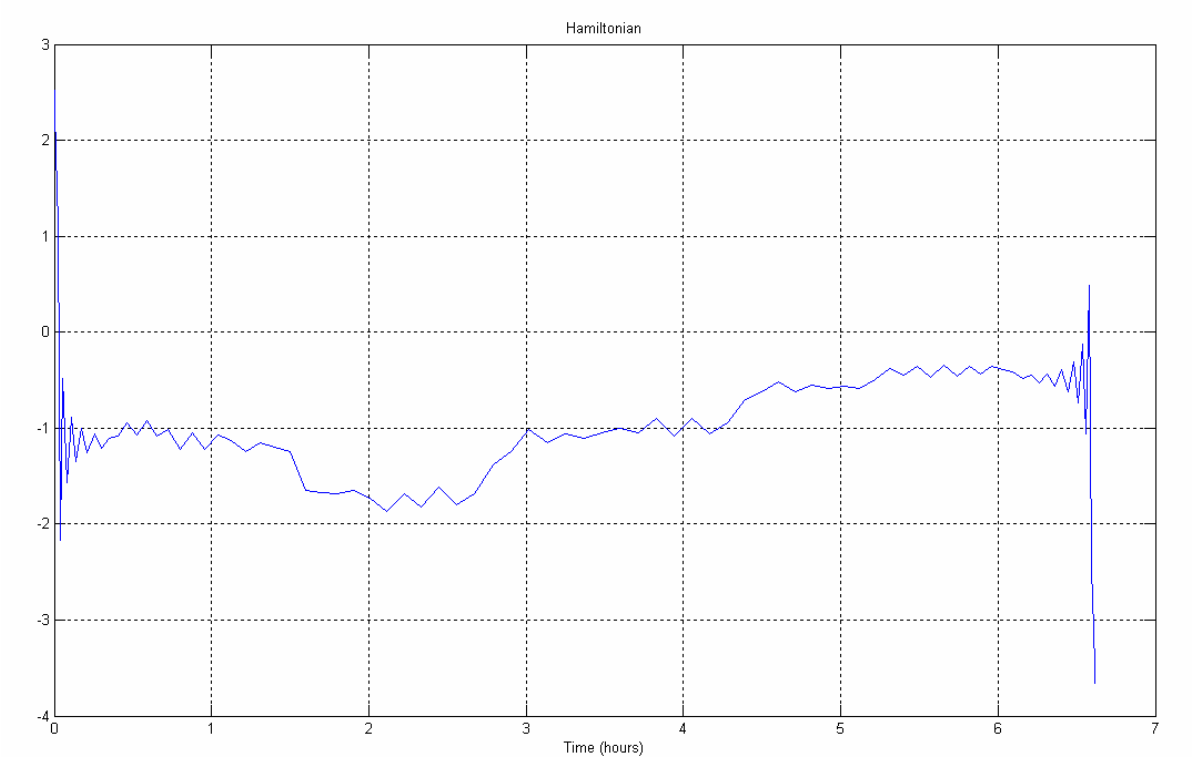

Figure 22. Problem (T): Hamiltonian Evolution and Value Condition Satisfied

e. Terminal Transversality Condition

Boundary conditions on the costates do match expected theoretical values and confirm optimal control theory, in that free terminal boundary states have corresponding costates of zero (x_4 = right ascension of ascending node, x_5 = argument of perigee, x_6 = true anomaly)and the state being maximized (e.g. x_1 = semimajor axis) has a corresponding terminal costate of -1. These conditions are listed in Table 7.

$\lambda_a = \frac{\partial \overline{E}}{\partial a_f} = \nu_a$	$\lambda_\Omega = \frac{\partial \overline{E}}{\partial \Omega_f} = 0$
$\lambda_e = \frac{\partial \overline{E}}{\partial e_f} = \nu_e$	$\lambda_\omega = \frac{\partial \overline{E}}{\partial \omega_f} = 0$
$\lambda_i = \frac{\partial \overline{E}}{\partial i_f} = \nu_i$	$\lambda_\nu = \frac{\partial \overline{E}}{\partial \nu_f} = 0$

Table 7. Terminal Transversality Conditions

A plot of the costates with respect to time also illustrates satisfactory compliance with the expected Transversality conditions. As expected, the λ_Ω ,λ_ω and λ_ν terminal values are 0.

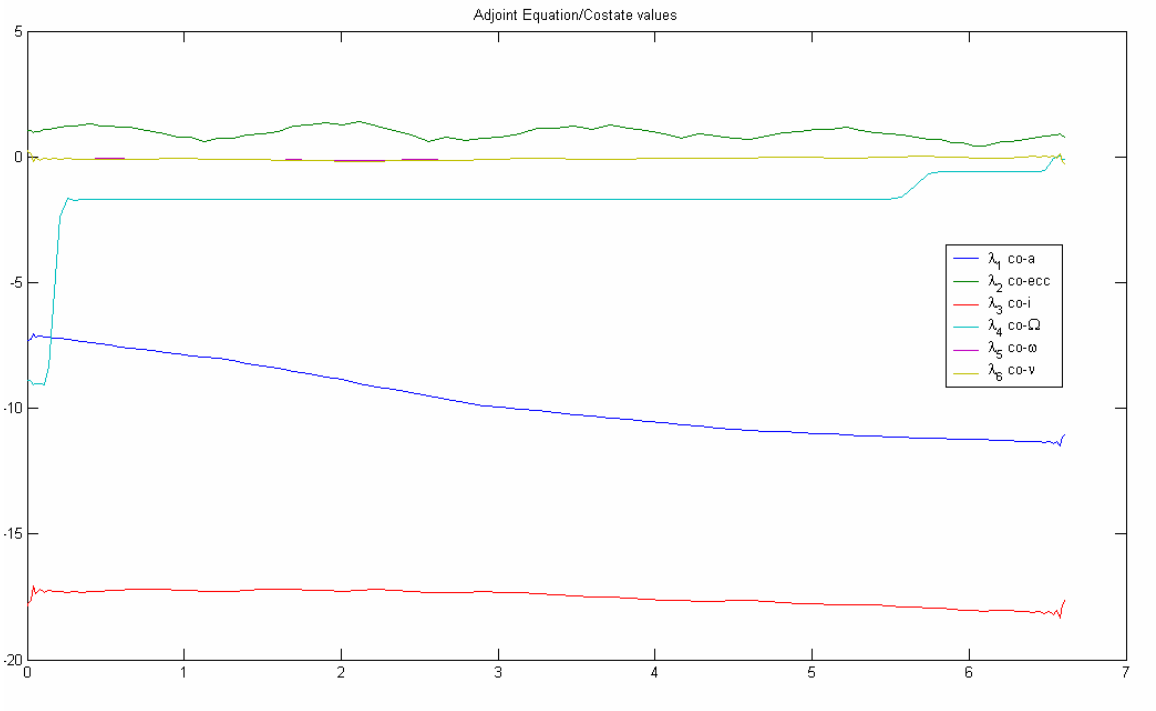

Figure 23. Problem (T): Terminal Transversality Condition Satisfied

D. VARIATION: PROBLEM (D)

A variation of Problem (T) is provided to demonstrate the flexibility of the problem formulation and as a second opportunity for model verification. The orbital debris mitigation application discussed earlier is modeled by adapting the Problem (T) formulation to "transfer" from the initial 339km orbit to a zero-altitude orbit in minimum time. This deorbit variation is designated Problem (D).

1. Problem Formulation

Problem (D) simply modifies the formulation presented earlier:

$$\text{Problem(D)}\begin{cases}\text{Minimize } J[\mathrm{x}(\cdot),\,\mathrm{u}(\cdot),\,t_f]=t_f\\ \text{Subject to}\quad \dot{\mathrm{a}}=(2a^2/h)[e\sin(\nu)\,f_r+(p/r)\,f_\theta]\\ \qquad\qquad \dot{\mathrm{e}}=(1/h)\{p\sin(\nu)\,f_r+[(p+r)\cos(\nu)+re]\,f_\theta\}\\ \qquad\qquad \mathrm{i}=(r\cos(\omega+\nu)/h)\,f_h\\ \qquad\qquad \dot{\Omega}=(r\sin(\omega+\nu)/h\sin(i))\,f_h\\ \qquad\qquad \dot{\omega}=(1/he)[-p\cos(\nu)\,f_r+(p+r)\sin(\nu)\,f_\theta]\\ \qquad\qquad\qquad -[r\sin(\omega+\nu)\cos(i)/h\sin(i)]\,f_h\\ \qquad\qquad \dot{\nu}=h/r^2+[(1/eh)[p\cos(\nu)\,f_r-(p+r)\sin(\nu)\,f_\theta]\\ (a_0,\ e_0,\ i_0,\ \Omega_0,\omega_0,\nu_0)\ =\ (6717km,0.02,51.59^o,0^o,50^o,0^o)\\ \qquad (a_f)\ =\ (6378km)\end{cases}$$

The terminal endpoint manifold for the state vector only has one equality constraint, a_f. System dynamics and cost function remain the same as described for Problem (T). As was the case for the first problem, the optimal control produced by DIDO was interpolated and used to propagate the dynamic equations from the initial state vector. Figures 24-31 show feasibility and the totality of necessary conditions for optimality. In particular, Figures 24-29 demonstrate feasibility as the propagated states correspond to the DIDO produced vector.

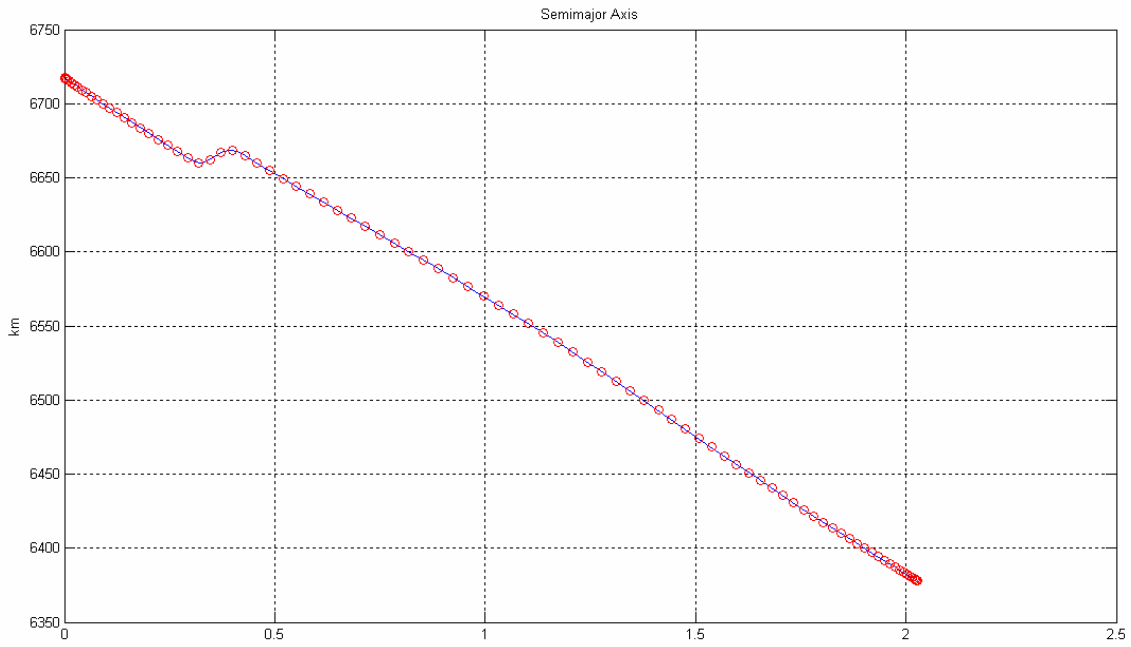

Figure 24. Problem (D): Feasibility demonstrated in semimajor axis (90 nodes employed)

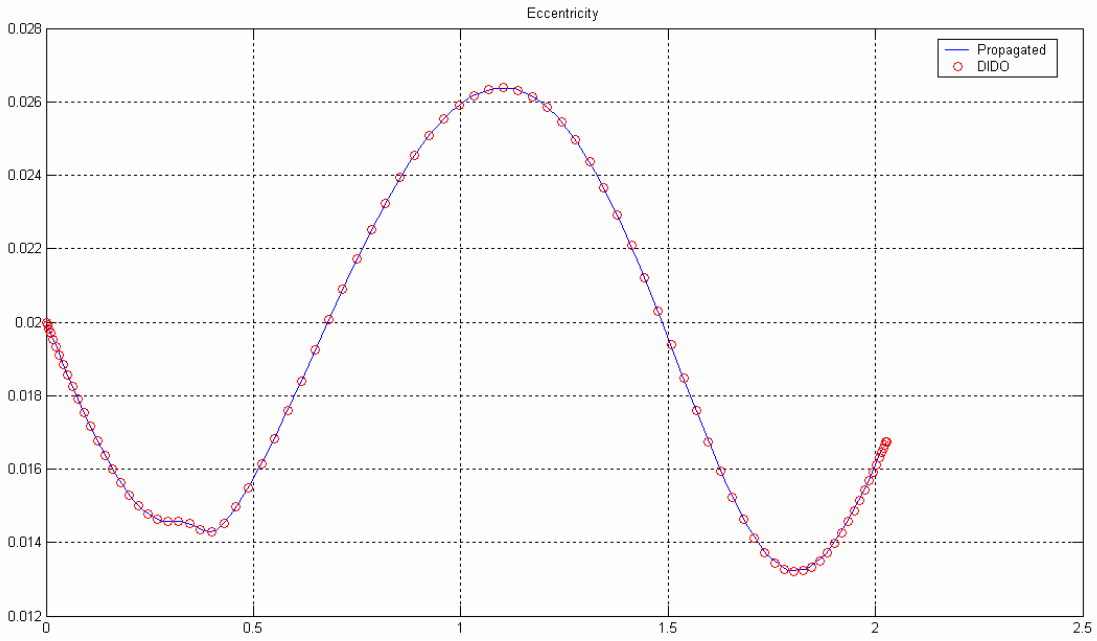

Figure 25. Problem (D): Feasibility demonstrated in Eccentricity (90 nodes employed)

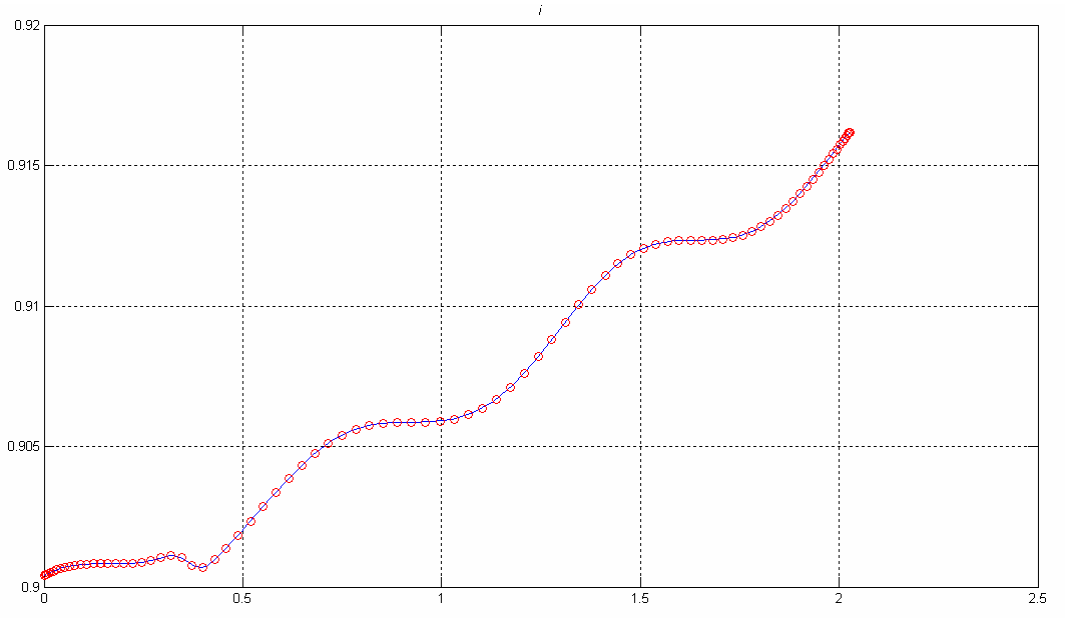

Figure 26. Problem (D): Feasibility demonstrated in Inclination (90 nodes employed)

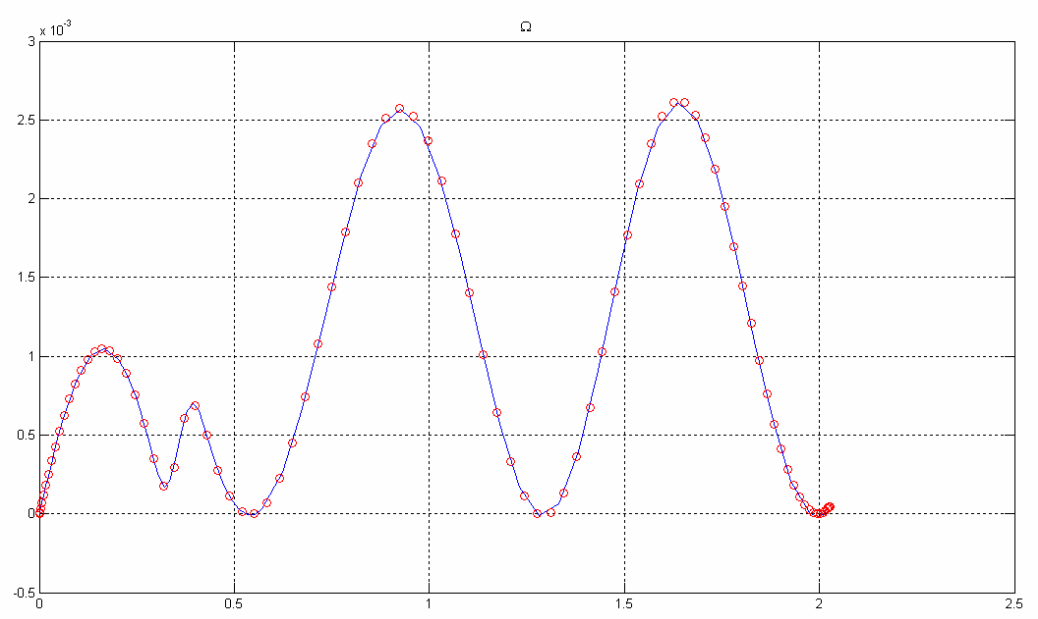

Figure 27. Problem (D): Feasibility demonstrated in RAAN (90 nodes employed)

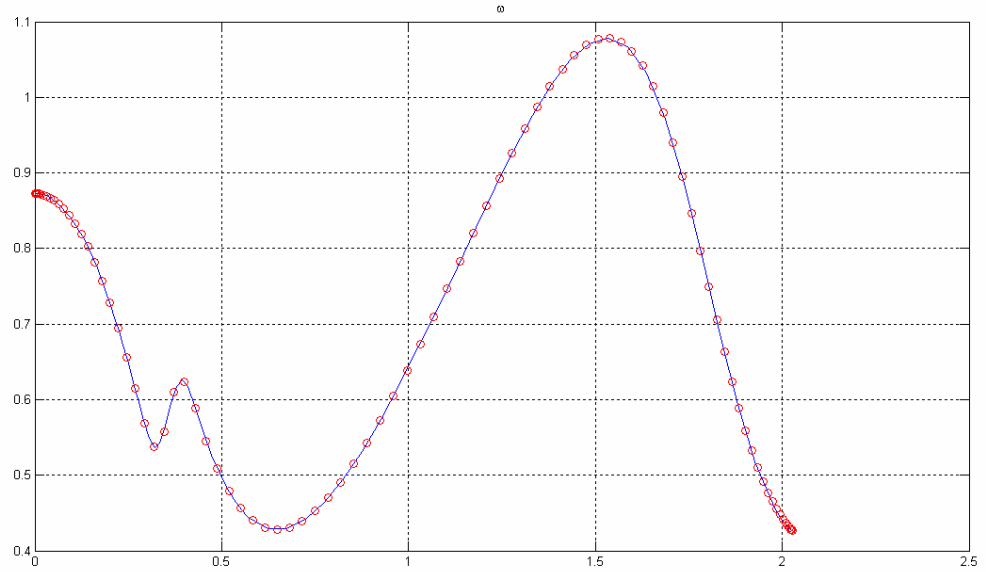

Figure 28. Problem (D): Feasibility demonstrated in Argument of Perigee (90 nodes employed)

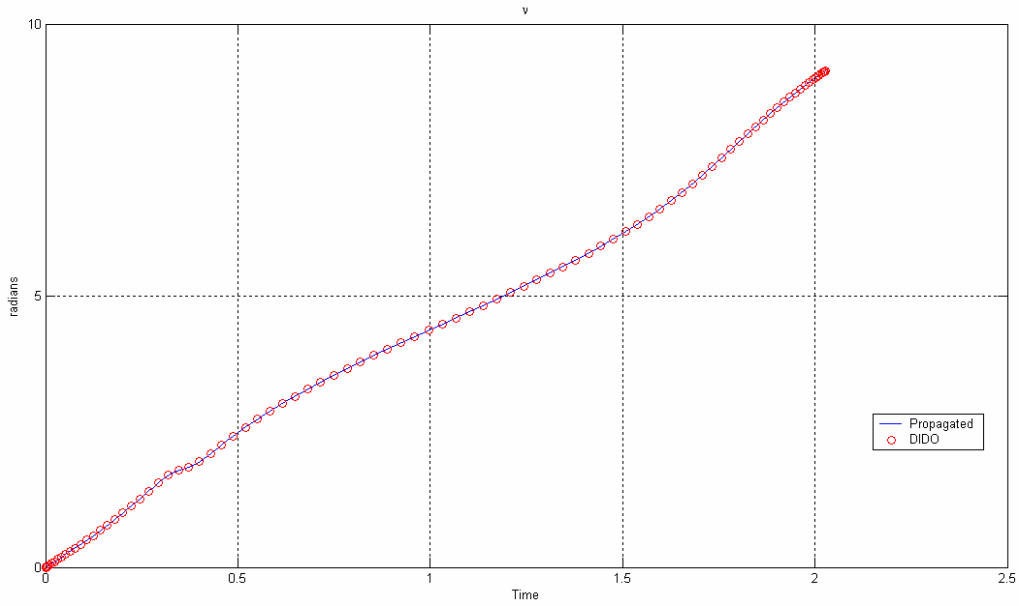

Figure 29. Problem (D): Feasibility demonstrated in true anomaly (90 nodes employed)

The necessary conditions for optimality are met: Problem (D) has the calculated conditions for the Hamiltonian Evolution Equation as $\dot{H} = 0$ and the Hamiltonian Value Condition as $H\left[t_f\right] = -\dfrac{\partial \overline{E}}{\partial t} = -1$. These conditions are evident in Figure 30.

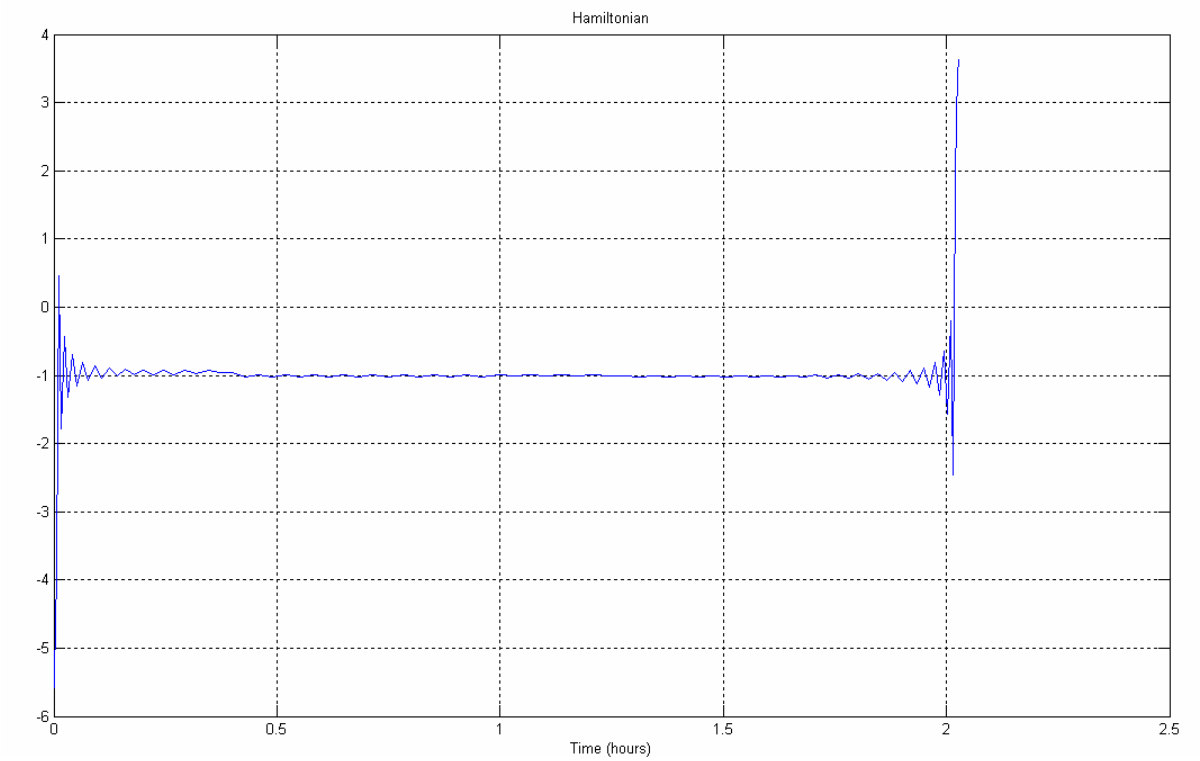

Figure 30. Problem (D) Hamiltonian (90 nodes)

Finally, the costate dynamics are presented in Figure 31 on the following page. As evident from the final values of the costates, these correspond to the Terminal Transversality Conditions for Problem (D):

$\lambda_a = \dfrac{\partial \overline{E}}{\partial a_f} = \nu_a$	$\lambda_\Omega = \dfrac{\partial \overline{E}}{\partial \Omega_f} = 0$
$\lambda_e = \dfrac{\partial \overline{E}}{\partial e_f} = 0$	$\lambda_\omega = \dfrac{\partial \overline{E}}{\partial \omega_f} = 0$
$\lambda_i = \dfrac{\partial \overline{E}}{\partial i_f} = 0$	$\lambda_\nu = \dfrac{\partial \overline{E}}{\partial \nu_f} = 0$

Table 8. Problem (D) Terminal Transversality Conditions

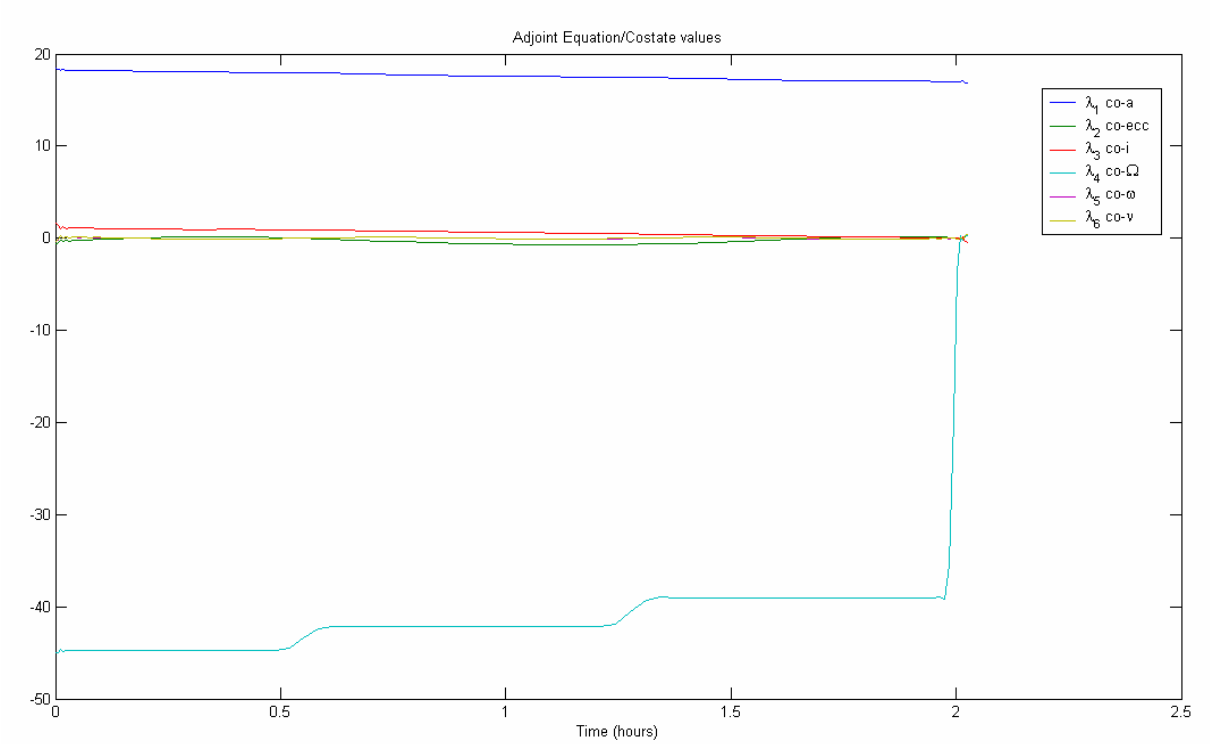

Figure 31. Problem (D) Costates (90 nodes)

E. CONCLUSIONS: PROBLEMS (T) AND (D)

1. Solution

Model feasibility is verified, and the totality of necessary conditions for optimality was considered. Problem (T) as shown presents a feasible solution to the optimal control desired for an orbit transfer via induced force from a current-carrying tether. The orbit transfer considered involved altitude raising and a terminal manifold requiring return to initial eccentricity and inclination values. Problem (D) likewise presents a feasible solution to the optimal control desired for a deorbit maneuver. The deorbit maneuver considered used a terminal manifold with semimajor axis equal to the earth radius and all other state variables free.

2. Shortfalls

Problem (T) is ready for additional complexities. An exploration of possible initial and terminal manifolds with respect to orbit transfers can lead to a developed reachable set of transfer control algorithms. Initial steps towards increasing the complexity of Problem (T) include development of "target" final orbits, increasing the

event constraints for the orbital maneuver. Additionally, the disparity between calculated theoretical values and computationally derived values in the case of the Hamiltonian requires further review as the differences are not immediately attributable to computational error alone. Furthermore, the absence of a developed model for tether librations not only deprives this formulation of a significant increase in fidelity but also restricts the tether dynamics. Either a set of static off-nadir tether perturbations or merely two dimensions of perturbation accelerations are available from a rigidly nadir-oriented tether vice the full 3-DOF control available for a librating tether.

Another deficit from the author's viewpoint is the absence of "target resolution" via applying Bellman's Principle of Optimality. Following Bellman, for a given optimal solution, the same terminal manifold should be achieved regardless of starting point, provided the starting node is on the optimal solution path. Solving the optimal solution from different starting points (nodes) within the current optimal solution would verify the assumption of a developed bang-bang control with the increase in resolution afforded by the increase in discrete data points. This is an especially helpful technique in analysis of DIDO-generated solutions, as the nodes appear more frequently at initial and terminal manifolds. Starting a "new solution" from an interior node will provide more resolution for the optimal solution, in addition to validating the original solution, in that the same optimal path should be followed from starting at any node on the original optimal path. An examination of Bellman's Principle could then be followed by an evaluation of the Value function and development of a cost surface for the problem formulation. Other recommendations for future work beyond the optimal control facets of Problem (T) or Problem (D) are discussed in the next chapter.

THIS PAGE INTENTIONALLY LEFT BLANK

V. FUTURE WORK

A. MINIMIZING ASSUMPTIONS

Other than the shortfalls mentioned in the previous section, further problem formulation improvements should begin with dynamic models. The Legendre polynomial model for the Earth Magnetic (B) field as employed by Lanoix, et al,[42] should replace the simpler linear model used by Williams and this study. The state vector used here should be transformed into equinoctial elements for optimality and propagation, thereby reducing potential for singularities due to low inclination and eccentricity values.

B. TECHNOLOGY GROWTH

The material properties of tethers in use have significant implications to optimal orbit maneuvers, especially with regard to the feasible set of maneuvers. Lanoix, et. al., briefly compare the bare-wire tether with the sheathed tether. In addition to recommending the obvious continuation of tether material and structure development, we recommend incorporation of tether conductivity into the dynamic model. Paired with a more robust magnetic field simulation, permutations of tether systems based on a variable percentage of tether length as bare-wire could be optimized in conjunction with applied current or even tether length.

A very real drawback to the use of a tether system for both of the scenarios described is the extreme frailty of the tether itself. Several actual tether tests deployed from the space shuttle have failed within days because the tether was severed by small orbiting debris. An intensive study on tether survivability after impact with manmade debris and micrometeoroids (MM) was conducted by Penson and Burchell of the University of Kent.[43] The study was based on six month missions in both LEO and GEO, employing a 500 m long and 1 mm thick tether. Various materials (Dyneema,

[42] Eric L. M. Lanoix, Arun K. Misra, Vinod J. Modi, and George Tyc. "Effect of Electrodynamic Forces on the Orbital Dynamics of Tethered Satellites". *Journal of Guidance, Control, and Dynamics*, Vol. 28, No. 6, November-December 2005.

[43] James S. G. Penson and Mark Burchell, "Hypervelocity Impact Studies on Space Tethers," IAC-03-I.5.04, IAF Bremen 2003.

Kevlar and Aluminum) and layers were evaluated against different size MM's in order to determine the most suitable configuration of material and layers; results are shown in Figures 17 and 18 on the following page. Dyneema is a strong light weight material made from ultra high molecular weight polyethylene. Debris velocity in LEO and GEO was taken to be 14 km/s and 100-500 m/s respectively.

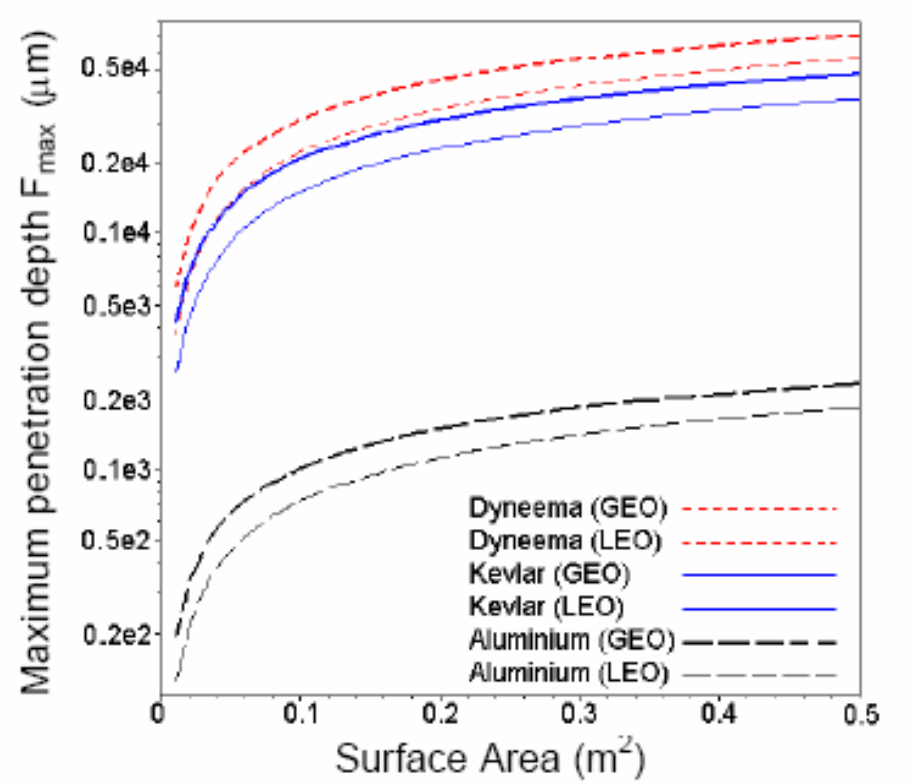

Figure 32. Max Penetration Depth as a Function of Surface Area (from Ref. 27)

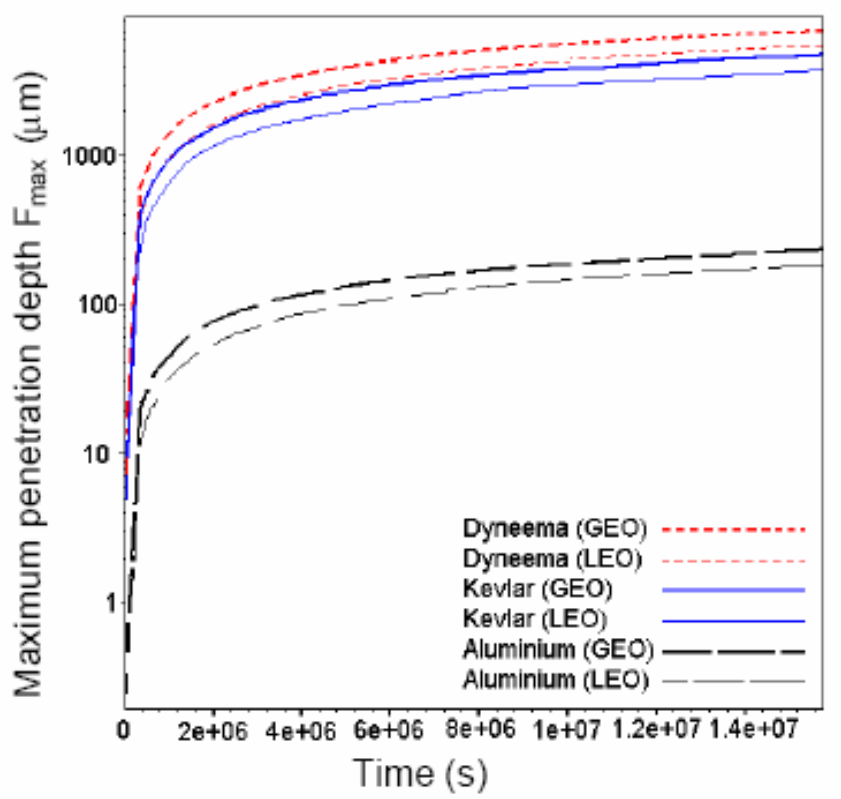

Figure 33. Max Penetration Depth as a Function of Time (from Ref. 27)

The figure on the previous page show that the maximum penetration for the Al target in LEO and GEO for six months is 0.15 -0.2 mm, while the Kevlar and Dyneema suffered 3-5 mm penetrations. The 1 mm strands of Kevlar and Dyneema would lasts only days in orbit, while the 0.3 mm strands of triple layer Aluminum (Al) would survive the impact of the tested 254 µm projectile with a 5 km/s velocity. The triple-layer Al strand (Figure 19) was effective with projectile diameters up to 500 µm; however, larger particles severed the strand. The survivability of the tether is the limiting factor that will prevent its large-scale utilization in the near future.

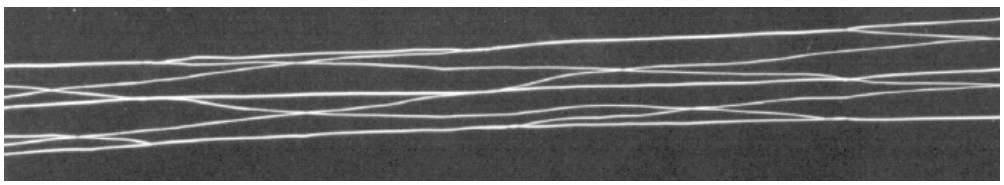

Figure 34. Knitted Al Wire Tether (from Ref. 27)

In addition to the potential disastrous effects of a tether-particle collision, EDT's face other electromechanical problems. As mentioned, more than one experimental tether has failed due to the tether not surviving deployment of the system. The tether has either failed to deploy or has snapped upon reaching full extension. Moreover, the tethers often experience high, fluctuating voltages in space which can produce serious mechanical vibrations. The vibrations are due to fluctuations in induced voltages from magnetic field as well as varying electron densities. The extremely long moment arms of the tether can result in forces which make a tether system dynamically unstable.

C. OPTIMAL VARIATIONS

Equipped with a functionally verified dynamic model, the robust capability of the dynamic optimization software package DIDO allows for ready optimization of any parameters contained in the current model. For example, in our system tether length is constant; however a combination of tether length and current could be employed in an optimal control scheme where now $\underline{u} = \left[tether_{current}, tether_{length} \right]$; $U = R^2$ providing more robust control, possibly expanding the feasibility set of orbital maneuvers using electrodynamic tethers. Williams, et al., touch upon an increased control complexity through incorporating a mission function control law that uses both tether tension and electromagnetic force scheduling (via current) to control librations and it is inferred also manipulate orbital elements. Incorporation of these more robust formulations can only increase the likelihood of successful on orbit testing for a fully operational program and test plan.

Furthermore, the accuracy of modern propagation techniques can eventually be considered in the optimal control development. For instance, the known orbital characteristics of a satellite can be programmed out for the life cycle of the system, so that element sets for the on orbit lifetime are known. This information could be incorporated into an optimization routine to determine not only the optimal control current and tether length required to implement a maneuver, but could delineate the optimal execution time dependent upon the specific cost function employed in the optimization routine.

D. PROGRAM DEVELOPMENT

The absence of a viable electrodynamic tether program cannot be discounted as a hindrance to concept maturation. Delays and cancellations of on-orbit system testing have allowed the development of a repository of research questions that require testing in space, an environment with which simulations and modeling cannot compare. A small test satellite with a focused mission should be developed to validate or disprove the recent flurry of simulations and analyses. Despite the over 5 year gap since an operational tether was last flown, the scientific community and space industry has continued to research and investigate the feasibility and optimality of electrodynamic tethers on orbit; the list of potential applications only increases. The thought of how much faster the state of the art could progress given viable test data from a robust and healthy program is exhilarating and challenging, to say the least. Whether economic or scientific the benefits of pushing forward in the important research area of electrodynamic tethers cannot be overstated.

THIS PAGE INTENTIONALLY LEFT BLANK

LIST OF REFERENCES

1. Vallado, David A. *Fundamentals of Astrodynamics and Applications, 2nd ed.* 2001: Microcosm Press, El Segundo, CA, pp. 158-165.

2. Bate, Roger R., Donald D. Mueller, and Jerry E White. Fundamentals of Astrodynamics. 1971: Dover Publications, Inc, New York. pp. 397-398.

3. Halliday, David. Robert Resnick, and Jearl Walker. *Fundamentals of Physics, Sixth Ed.*2001: Wiley & Sons, Inc. pp. 104-106.

4. Mishne, David. *Formation Control of Satellites Subject to Drag Variations and J_2 Perturbations,* Journal of Guidance, Control, and Dynamics, Vol. 27. No 4, July-August 2004.

5. Forward, Robert L and Robert P. Hoyt, *Terminator Tether TM: A Spacecraft Deorbit Device.* Journal of Spacecraft and Rockets Vol. 37, No. 2, March-April 2000. American Institute of Aeronautics and Astronautics. Amplifying information and figures obtained from http://www.tethers.com, accessed 10 Feb 2006.

6. Tragresser, Steven G., and Hakan San, "Orbital Maneuvering with Electrodynamic Tethers," *Journal of Guidance, Control, and Dynamics*, Vol. 26, No. 5, 2003.

7. Williams, Paul." Optimal Orbital Transfer with Electrodynamic Tether," *Journal of Guidance, Control, and Dynamics,* Vol. 28, No. 2, March-April 2005. American Institute of Aeronautics and Astronautics.

8. Parkinson, W.D., *Introduction to Geomagnetism*. Elsevier Science Pub. Co., Inc., New York.

9. Lanoix, Eric L. M., Arun K. Misra, Vinod J. Modi, and George Tyc. "Effect of Electrodynamic Forces on the Orbital Dynamics of Tethered Satellites". *Journal of Guidance, Control, and Dynamics,* Vol. 28, No. 6, November-December 2005.

10. Johnson, L. "The Tether Solution," *IEEE Spectrum*, Vol. 37, No. 7, July 2000. National Aeronautics and Space Administration.

11. Vas, Irwin E., Thomas J. Kelly, and Ethan A Scarl, "Space Station Reboost with Electrodynamic Tethers," *Journal of Spacecraft and Rockets,*Vol. 37, No. 2, March-April 2000. American Institute of Aeronautics and Astronautics.

12. Cosmo, M.L. and E. C. Lorenzini, *Tethers in Space Handbook, 3rd ed.,* NASA Marshall Space Flight Center Grant NAG8-1160. 1997.

13. Lanoix, Eric L. M., Arun K. Misra, Vinod J. Modi, and George Tyc. “Effect of Electrodynamic Forces on the Orbital Dynamics of Tethered Satellites”. *Journal of Guidance, Control, and Dynamics*, Vol. 28, No. 6, November-December 2005.

14. Hoyt, R. P., “Stabilization of Electrodynamic Space Tethers,” *Proceedings of Space Technology and Applications International Forum (STAIF-2002),* American Institute of Physics, Melville NY, 2002, pp. 570-577

15. Six, Dr. Frank. National Space Science Data Center, National Aeronautics and Space Administration Marshall Space Flight Center, Huntsville, AL, Master Catalog display (spacecraft) website updated 09 Nov 2005, accessed 10 Feb 2006. http://nssdc.gsfc.nasa.gov/database/MasterCatalog?sc=TSS-1.

16. Bray, Becky and Patrick Meyer, editors. “Liftoff to Space Exploration,” archived website hosted by National Aeronautics and Space Administration, website accessed 10 Feb 2006. http://liftoff.msfc.nasa.gov/shuttle/sts-75/tss-1r/tss-1r.html.

17. Grossi, M. D., and E. McCoy, "What Has Been Learned in Tether Electrodynamics from the Plasma Motor Generator (PMG) Mission on June 1993," ESA/International Round Table on Tethers in Space, ESTEC Conference Centre, Noordwikj, The Netherlands, 28-30 September 1994.

18. Lorenzini, E. and Juan Sanmartin, “Electrodynamic Tethers in Space,” *Scientific American,* August 2004.

19. http://cfa-www.harvard.edu/~spgroup/missions.html, accessed 10 Feb 2006.

20. http://www.spacetoday.org/images/Rockets/FutureSpaceVehicles/SailProSEDS.jpg, accessed 10 Feb 2006.

21. Pelaez, J., and Y. N. Andres, “Dynamic Stability of Electrodynamic Tethers in Inclined Elliptical Orbits,” *Journal of Guidance, Control, and Dynamics*, Vol. 28, No. 4, July-August 2005. American Institute of Aeronautics and Astronautics.

22. Somenzi, L., L. Iess, and J. Pelaez, “Linear Stability Analysis of Electrodynamic Tethers,” *Journal of Guidance, Control, and Dynamics*, Vol. 28, No. 5, September-October 2005. American Institute of Aeronautics and Astronautics.

23. Mankala, Kalyan, and Sunil K. Agrawal, “Equilibrium-to-Equilibrium Maneuvers of Rigid Electrodynamic Tethers,” *Journal of Guidance, Control, and Dynamics*, Vol. 28, No. 3, May-June 2005. American Institute of Aeronautics and Astronautics.

24. Williams, Paul, Takeo Watanbe, Chris Blanksby, Pavel Trivailo, and Hironori A. Fujii, “Libration Control of Flexible Tethers Using Electromagnetic Forces and Movable Attachment,” *Journal of Guidance, Control, and Dynamics*, Vol. 27, No. 5, September-October 2004. American Institute of Aeronautics and Astronautics.

25. Kechichian, J.A., "Trajectory Optimization Using Nonsingular Orbital Elements and True Longitude," *Journal of Guidance, Control, and Dynamics* Vol. 20, No. 5. 1997. American Institute of Aeronautics and Astronautics.

26. Mendy, Paul B., Maj., USAF, "Multiple Satellite Trajectory Optimization," December 2004 Master's Thesis, Naval Postgraduate School, Monterey, CA.

27. Penson, James S. G., and Mark Burchell, "Hypervelocity Impact Studies on Space Tethers," IAC-03-I.5.04, IAF Bremen 2003.

28. Ross, I. Michael. AE4850 Class notes, 2004. Naval Postgraduate School, Monterey, CA.

29. Ross, I. Michael and Fahroo, F. *User's Manual for DIDO 2003*. 2003. Naval Postgraduate School. NPS Technical Report MAE 03-005., Monterey, CA.

THIS PAGE INTENTIONALLY LEFT BLANK

INITIAL DISTRIBUTION LIST

1. Defense Technical Information Center
   Ft. Belvoir, VA

2. Dudley Knox Library
   Naval Postgraduate School
   Monterey, CA

3. Guidance, Navigation, and Control Laboratory
   Naval Postgraduate School
   Monterey, CA

4. Dr. I. M. Ross
   Naval Postgraduate School
   Monterey, CA

5. Dr. D. A. Danielson
   Naval Postgraduate School
   Monterey, CA

6. Dr. R. Panholzer
   Naval Postgraduate School
   Monterey, CA

7. LCDR Andrew Carlson
   Naval Postgraduate School
   Monterey, CA